9-6-2023

Single genomic enhancers drive experience-dependent GABAergic plasticity to maintain sensory processing in the adult cortex

Ori Roethler

Eran Zohar

Katayun Cohen-Kashi Malina

Lidor Bitan

Harrison Wren Gabel

See next page for additional authors

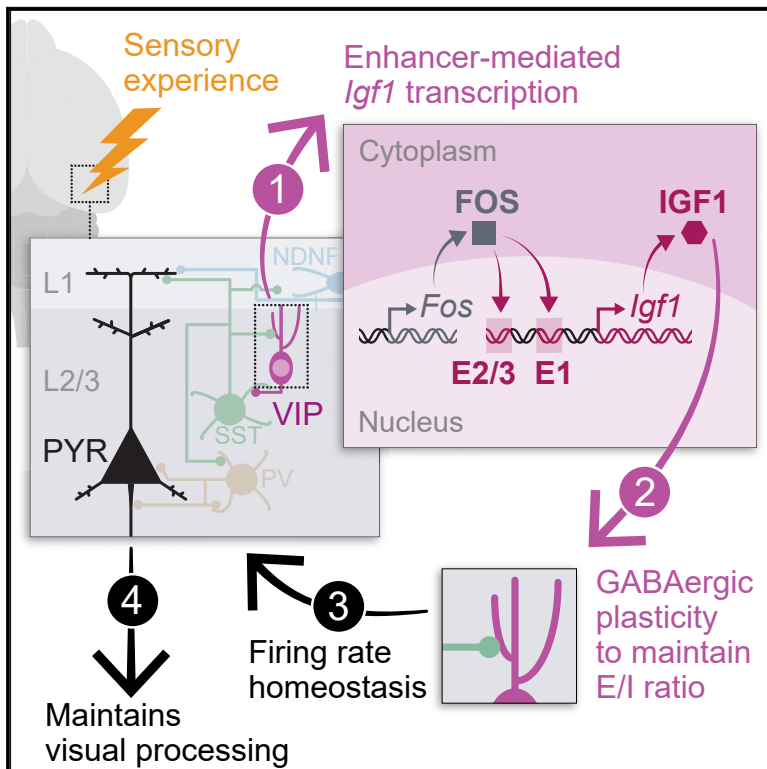## Authors

Ori Roethler, Eran Zohar, Katayun Cohen-Kashi Malina, Lidor Bitan, Harrison Wren Gabel, and Ivo Spiegel

Single genomic enhancers drive experience-dependent GABAergic plasticity to maintain sensory processing in the adult cortex

Graphical abstract

Authors

Ori Roethler, Eran Zohar,
Katayun Cohen-Kashi Malina,
Lidor Bitan, Harrison Wren Gabel,
Ivo Spiegel

Correspondence

ivo.spiegel@weizmann.ac.il

In brief

By identifying two enhancers that cooperatively drive experience-induced *Igf1* transcription in mouse cortical VIP interneurons and by analyzing the synaptic and circuit functions of these enhancers, Roethler et al. demonstrate that single experience-induced enhancers maintain information processing in adult neural circuits by modulating E/I ratio to homeostatically restrict neural activity.

Highlights

- Two enhancers drive activity-induced Igf1 transcription in VIP INs in mouse cortex

- Activity-induced Igf1 transcription drives GABAergic plasticity to maintain E/I ratio

- Activity-induced Igf1 enhancers restrict neural activity in VIP INs and PYR neurons

- Activity-induced Igf1 enhancers maintain visual processing in VIP INs and PYR neurons

CelPress

Neuron

Article

Single genomic enhancers drive experience-dependent GABAergic plasticity to maintain sensory processing in the adult cortex

Ori Roethler,[1,2,4] Eran Zohar,[1,2,4] Katayun Cohen-Kashi Malina,[1,2] Lidor Bitan,[1] Harrison Wren Gabel,[3] and Ivo Spiegel[1,2,5,*]

[1]Department of Brain Sciences, Weizmann Institute of Science, Rehovot, Israel
[2]Department of Molecular Neuroscience, Weizmann Institute of Science, Rehovot, Israel
[3]Department of Neuroscience, Washington University School of Medicine, St. Louis, MO, USA
[4]These authors contributed equally
[5]Lead contact
*Correspondence: ivo.spiegel@weizmann.ac.il
https://doi.org/10.1016/j.neuron.2023.05.026

SUMMARY

Experience-dependent plasticity of synapses modulates information processing in neural circuits and is essential for cognitive functions. The genome, via non-coding enhancers, was proposed to control information processing and circuit plasticity by regulating experience-induced transcription of genes that modulate specific sets of synapses. To test this idea, we analyze here the cellular and circuit functions of the genomic mechanisms that control the experience-induced transcription of Igf1 (insulin-like growth factor 1) in vasoactive intestinal peptide (VIP) interneurons (INs) in the visual cortex of adult mice. We find that two sensory-induced enhancers selectively and cooperatively drive the activity-induced transcription of Igf1 to thereby promote GABAergic inputs onto VIP INs and to homeostatically control the ratio between excitation and inhibition (E/I ratio)—in turn, this restricts neural activity in VIP INs and principal excitatory neurons and maintains spatial frequency tuning. Thus, enhancer-mediated activity-induced transcription maintains sensory processing in the adult cortex via homeostatic modulation of E/I ratio.

INTRODUCTION

Experience-dependent plasticity of synapses is required for an animal's ability to learn from and adapt to its environment[1,2] and thus is essential for its survival. Research over several decades has revealed that gene transcription in response to neuronal activity and sensory experience is a key molecular mechanism that underlies sensory experience-driven changes in synapses and behaviors.[3–6] Because gene transcription requires sequence-specific binding of transcription factors (TFs) to regulatory sites in the genome (e.g., enhancers and promoters), these regulatory sites are thought to control the experience-induced transcription of genes that modulate specific sets of synapses to thereby drive the experience-induced changes in neural circuit function that generate adaptive behaviors. However, although a wealth of experience-regulated non-coding genomic regulatory sites were identified[7–9] and enhancers were found to be enriched for mutations associated with neuropsychiatric disorders,[10–12] this idea remains untested: only a few experience-regulated genomic regulatory sites have been assessed for their ability to mediate experience-induced transcription,[13,14] and the role of enhancers in regulating synaptic and neural circuit plasticity remains largely unexplored.

Sensory experience and the subsequent increase in neural activity induce the transcription of a small and ubiquitous set (15–20 genes) of early-induced TFs[3,4] within minutes. These early-induced TFs, together with other (cell-type-specific) DNA-binding molecules, bind to specific enhancers and promoters to activate in each type of neuron the transcription of cell-type-specific sets of (hundreds of) late-induced effector genes, which alter the properties of cells and synapses. Thus, sensory-induced transcription is thought to modulate the flow and storage of information in neural circuits[15–19] and to contribute to adaptive behaviors.[20–26] Notably, most effector genes are transcribed to some degree also under basal conditions when the respective experience or stimulus is absent[27–29]; yet, nearly all of the studies that assessed their neurobiological functions manipulated the basal and experience-induced expression of the respective gene(s) instead of manipulating only the experience-induced changes in transcription. Thus, although it is clear that experience-induced genes have important neurobiological functions, the synaptic and circuit plasticity function selectively of their experience-induced transcription remains unknown.

In the cortex, experience-regulated gene programs include genes whose expression at peak induction is highly enriched
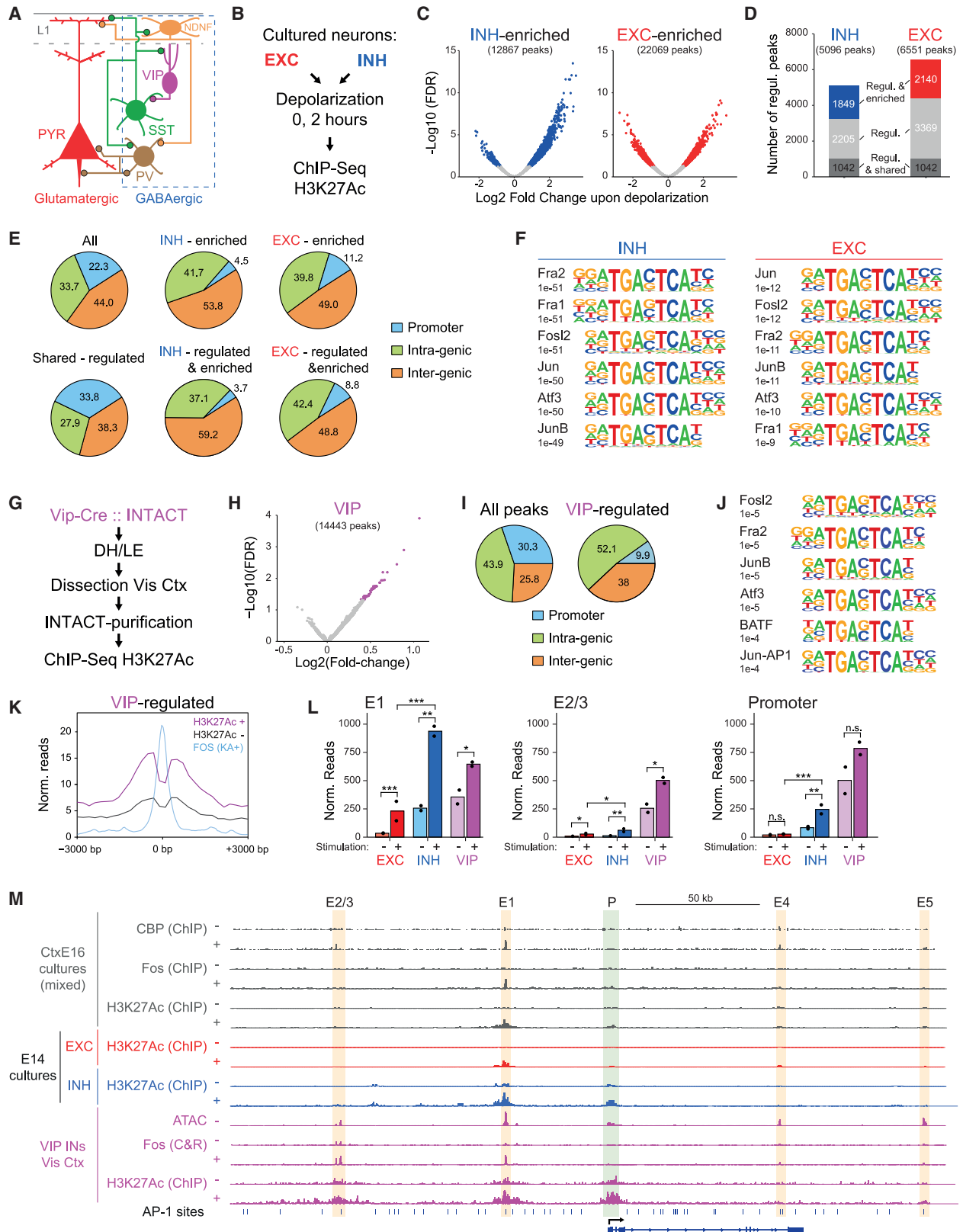
(legend on next page)

in only one cell type,[17,27,28] and many of these cell-type-specific and experience-induced genes encode for secreted signaling molecules, which modulate specific sets of synapses: for example, transcription of the gene encoding the insulin-like growth factor 1 (*Igf1*) is highly enriched and induced upon sensory stimulation in GABAergic interneurons (INs) that express the vasoactive intestinal peptide (VIP), and VIP IN-derived IGF1 promotes in the developing visual cortex inhibition onto VIP INs in a local and cell-autonomous manner.[27] Because VIP INs specialize in disinhibiting local excitatory neurons[30–32] (Figure 1A), induction of *Igf1* in VIP INs is expected to reduce the activity rates of VIP INs which, in turn, might reduce the activity rates of neighboring excitatory neurons. This idea remains untested, but because (1) VIP IN-derived IGF1 in the developing visual cortex controls the development of spatial frequency tuning in an experience-dependent manner,[27] and (2) VIP INs regulate plasticity in adult cortical circuits,[33–35] this suggests that the sensory-induced upregulation of *Igf1* in VIP INs in the adult visual cortex maintains activity rates in a homeostatic manner. Because the sensory-induced transcription of *Igf1*, similar to other sensory-induced genes, likely is mediated by sensory-dependent genomic regulatory sites, this suggests that sensory processing and plasticity in the adult cortex are regulated directly by specific single enhancers and/or promoters.

Here, we focus on *Igf1* in VIP INs in the adult visual cortex to analyze the cellular and circuit function of specific experience-induced enhancers. We find that sensory-driven transcription of *Igf1* in VIP INs is driven cooperatively by two cell-type-specific experience-induced enhancers, which promote inhibition onto VIP INs in a sensory-dependent manner. These enhancers maintain the ratio between excitation and inhibition (E/I ratio) in VIP INs to thereby restrict neural activity rates and maintain spatial frequency tuning in VIP INs and in principal excitatory neurons in the adult visual cortex. These findings indicate that sensory-induced transcription in the adult cortex maintains homeostatic control of sensory processing, thereby ensuring the cortex' functional integrity over time.

RESULTS

Cell-type-specific ChIP-seq for H3K27Ac identifies sensory-induced enhancers at the *Igf1* locus

The goal of our study was to determine the cellular and circuit function of sensory-induced transcription by focusing on the sensory-dependent genomic regulation of *Igf1* in VIP INs in the adult visual cortex. Because experience-induced transcription is mediated by enhancers and promoters, we first set out to map those genomic regulatory regions that drive selectively the sensory-induced transcription of *Igf1* in VIP INs. *Igf1* is expressed and activity-induced in a cell-type-specific manner in cultured GABAergic neurons[17,27] (Figure S1A) and in VIP INs in the adult visual cortex (Figure S1B); thus, these sites are expected to be more active in the respective cell types. Previous studies identified putative activity-regulated non-coding genomic sites near the *Igf1* locus, but these studies were either not done in a cell-type-specific manner,[36,37] lacked a (sensory) stimulation paradigm,[38,39] or were not analyzed to identify all sensory-induced changes in the chromatin landscape near the *Igf1* locus.[7] Thus, we took a comprehensive and unbiased approach to identify all activity-regulated (cell-type-specific) genomic sites in cultured inhibitory neurons and in cortical VIP INs to identify those enhancers near the *Igf1* locus that might drive the stimulation-induced upregulation of *Igf1* in these neurons.

To identify the genomic sites that are activity regulated in a cell-type-specific manner in cultured inhibitory neurons, we performed chromatin-immunoprecipitation followed by high-throughput sequencing (ChIP-seq) for H3K27Ac (a marker for transcriptionally active genomic sites[40,41]) on separate cultures of GABAergic or glutamatergic cortical neurons[17] that were stimulated with KCl-mediated depolarization[17,36,37,42] (Figure 1B). This identified 5,096 and 6,511 activity-regulated peaks in inhibitory and excitatory neurons, respectively. Comparison with the peaks enriched in either cell type (12,867 in inhibitory neurons, 22,067 in excitatory neurons; Figure 1C) revealed that 1,849 and 2,140 of the activity-regulated peaks are "regulated and

Figure 1. ChIP-seq for H3K27Ac identifies cell-type-specific sensory-regulated enhancers at the *Igf1* locus in cortical VIP INs

(A) Diagram of inhibitory circuitry in the mouse visual cortex (PYR, glutamatergic pyramidal excitatory neuron; PV/SST/VIP, GABAergic interneurons [INs] respectively expressing parvalbumin, somatostatin, and vasoactive intestinal protein).

(B) Experimental design for detecting cell-type-specific and activity-regulated genomic sites in cultured neurons.

(C) All H3K27Ac ChIP-seq peaks enriched either in GABAergic (INH) or glutamatergic (EXC) cultured neurons. Colored puncta represent sites with a FDR below 0.05 (blue, inhibitory; red, excitatory).

(D) Activity-regulated H3K27Ac ChIP-seq peaks in each cell type (FDR < 0.05) that are either enriched in a given cell type (regulated and enriched—colored), expressed and regulated in a similar manner (shared—dark gray), or expressed in both types of neurons but regulated only one of them (regulated—light gray).

(E) Genomic location of H3K27Ac peaks (numbers represent percentages).

(F) Enriched TFBS motifs (and respective p values) in putative enhancers for each cell type (see also Table S1).

(G) Experimental design for identifying sensory-regulated genomic sites in VIP INs in the adult visual cortex (data from GSE150538).

(H) Sensory-regulated H3K27Ac ChIP-seq peaks in visual cortex VIP INs (purple dots: FDR < 0.05).

(I) Genomic location of all H3K27Ac peaks (left) and of the 71 regulated peaks (right) in VIP INs (numbers represent percentages).

(J) Enriched TFBS motifs (and respective p values) in sensory-regulated peaks in VIP INs (see also Table S2).

(K) H3K27Ac ChIP-seq profiles before (black) and after (purple) light exposure, and Cut&Run binding of FOS (light blue) after stimulation (Kainic acid injections) centered around the ATAC-seq peaks detected within the 71 sensory-regulated peaks.

(L) Quantification of normalized reads before (−) or after (+) stimulation at the Igf1 promoter and putative regulated enhancers near the *Igf1* gene in each cell type (*<0.05, **<0.01, ***<0.001, Deseq2).

(M) Genome browser tracks of genomic data at the *Igf1* locus, including: cell-type-specific cortical cultures (INH and EXC, blue and red, respectively); mixed cortical cultures (gray)—ChIP-seq for H3K27Ac, CBP, and Fos; visual cortex VIPs (purple)—ChIP-seq for H3K27Ac, ATAC-seq, Cut&Run for Fos (−/+ stimulation). Putative enhancer regions are highlighted in yellow and the *Igf1* promoter in green.

enriched," respectively, in inhibitory and excitatory neurons (Figures 1C and 1D). Notably, the majority of the regulated peaks identified are either regulated in both types of neurons ("regulated and shared," Figure 1D) or regulated only in one type but also present in the other ("regulated," Figure 1D). Most of the identified peaks are located either inter- or intra-genic (Figure 1E), indicating that the majority of these genomic regions likely correspond to enhancers. This bias is even more pronounced in peaks that are "enriched" or "regulated and enriched" in the respective cell type, which is consistent with previous observations that cell-type-specific active genomic regulatory sites tend to be enhancers and not promoters.[43–45] Further analyses revealed that these genomic sites are highly enriched in both cell types for TF binding sites (TFBSs) of well-known stimulus-responsive TFs (Figure 1F; Table S1), including JUNB and FOSL2, which, together with the experience-induced TFs, FOS and JUN, can regulate stimulus-induced gene expression by forming part of the AP-1 complex.[37,46–48] Together, these findings characterize the cell-type-specific landscape of activity-regulated genomic sites in cultured inhibitory and excitatory neurons.

Next, we sought to identify sensory-regulated genomic sites in visual cortex VIP INs by analyzing datasets that were generated by H3K27Ac ChIP-seq on VIP IN nuclei isolated from the visual cortices of adult mice that were either dark-housed for 7–14 days (DH) or dark housed and then exposed to ambient light for 3 h (LE) (Figure 1G).[7] These analyses identified 14,443 H3K27Ac peaks in VIP INs, 71 of which were sensory regulated (Figure 1H; Table S4). Similar to cultured neurons, the vast majority of these sensory-regulated peaks are putative enhancers (64 of 71 peaks map to inter- or intra-genic sites; Figure 1I) and are enriched for binding sites of components of the AP-1 complex (Figure 1J; Table S2). Consistent with these observations, analyses of data generated by Cut&Run (C&R) for FOS on VIP IN nuclei isolated from the cortices of kainate-stimulated mice[7] revealed that FOS binds to 90.1% of these sensory-regulated sites, right in their middle (Figure 1K). Thus, because FOS preferentially binds to enhancers,[49] we conclude that most of these genomic sites are putative sensory-induced enhancers.

Having characterized genome-wide putative activity-regulated enhancers in cultured GABAergic neurons and cortical VIP INs, we next sought to identify those enhancers that might drive the activity-induced transcription of *Igf1*. For this, we focused on the *Igf1* locus and compared the sites that contain H3K27Ac ChIP-seq peaks in cultured inhibitory neurons and in visual cortex VIP INs with additional genomic datasets, including ChIP-seq for CBP, FOS, and H3K27Ac in stimulated mixed cortical cultures,[36,37] C&R for FOS in visual cortex VIP INs of kainate-stimulated mice, and ATAC-seq in VIP INs isolated from the visual cortices of standard-housed mice[38] (Figure 1M). This revealed three putative enhancers in which the H3K27Ac signal is stimulus-induced in cultured inhibitory neurons and in visual cortex VIP INs (Figure 1L) and which contain additional hallmarks of activity-regulated enhancers (e.g., ATAC-seq peaks, sensory-induced FOS-binding in visual cortex VIP INs). The proximal of these enhancers (E1) is located ~40 kb upstream of the *Igf1* transcriptional start site (TSS) (Figure 1M) and was identified in a previous study,[7] whereas the two distal enhancers (E2 and E3, ~100

kb upstream of the *Igf1* TSS) are adjacent to each other and were not identified in previous studies. Igf1 E2 and E3 are very close to each other and thus they likely act as one sensory-induced regulatory unit[50]; accordingly, we will refer to these enhancers as Igf1 E2/3. Notably, the ATAC-seq peaks at E1, E2, and E3 are cell type specific (Figure S1H), and the AP-1 sites at these enhancers are evolutionary conserved (Figure S1I; Table S3).[51] In addition to these three regulated enhancers, we identified two additional putative enhancers downstream of the *Igf1* TSS (E4 and E5, respectively 60 and 120 kb downstream) that are not regulated but contain hallmarks of active enhancers (i.e., CBP binding in cultured neurons, ATAC-seq peaks in VIP INs). Because the H3K27Ac signal at the regulated Igf1 enhancers (E1 and E2/3) is much stronger than that at the non-regulated enhancers (E4 and E5), these findings, together with the other genomic data, suggest that Igf1 E1 and E2/3 may drive the sensory-induced transcription of *Igf1* in VIP INs.

Igf1 enhancer 1 selectively controls the activity-induced transcription of *Igf1* in cultured inhibitory neurons

To assess whether the putative Igf1 enhancers identified by our genomic analyses drive stimulus-induced *Igf1* transcription, we first tested whether these enhancers could drive depolarization-induced gene expression in a luciferase enhancer reporter assay[37] in cultured neurons. Thus, we transfected reporter constructs containing the respective enhancer into cultured inhibitory neurons and compared luciferase activity before and after depolarization (Figure 2A). This revealed that only Igf1 E1 drives depolarization-induced gene expression in cultured GABAergic neurons (Figure 2B). Because E1 contains two canonical AP-1 sites (Figures S1G and S1I) and FOS regulates *Igf1* expression at least in part,[37] we next tested reporter constructs in which the AP-1 sites in E1 are deleted (Figure 2C). This revealed that both AP-1 sites are necessary for the full stimulus-induced transcriptional potential of E1 (Figure 2D). Thus, together with our genomic data, these findings indicate that E1 is the major depolarization-induced *Igf1* enhancer in cultured inhibitory neurons.

To test directly whether the activity-induced Igf1 enhancers identified in our genomic analyses (Igf1 E1 and E2/3) drive the activity-induced upregulation of *Igf1*, we generated three Cre-conditional knockout (cKO) mouse alleles in which either E1 is flanked by LoxP sites ("Igf1-E1 flox"), E2/3 is flanked by Lox2722 sites ("Igf1-E2/3 flox"), or E1 and E2/3 are, respectively, flanked by LoxP and lox2722 sites ("Igf1-E12/3 flox") (Figures S2A and S2B). As intended, these novel alleles allow for the selective removal of the respective enhancer(s), whereby Cre-recombination does not remove the genomic region between E1 and E2/3 in the Igf1-E12/3 flox mice (Figures S2C–S2F). Importantly, mice harboring these floxed alleles develop with normal bodyweight (Figure S2G) and the levels of *Igf1* in the visual cortex and other tissues of these mice are indistinguishable from those in wild-type (WT) littermates (Figure S2H); similarly, *Igf1* levels in cultured cortical neurons prepared from embryos homozygous for the Igf1-E1 flox allele or from control littermates are indistinguishable (Figure S2I). Thus, these mouse alleles are suitable for loss-of-functions experiments aimed at determining the transcriptional and biological function of Igf1 E1 and E2/3.
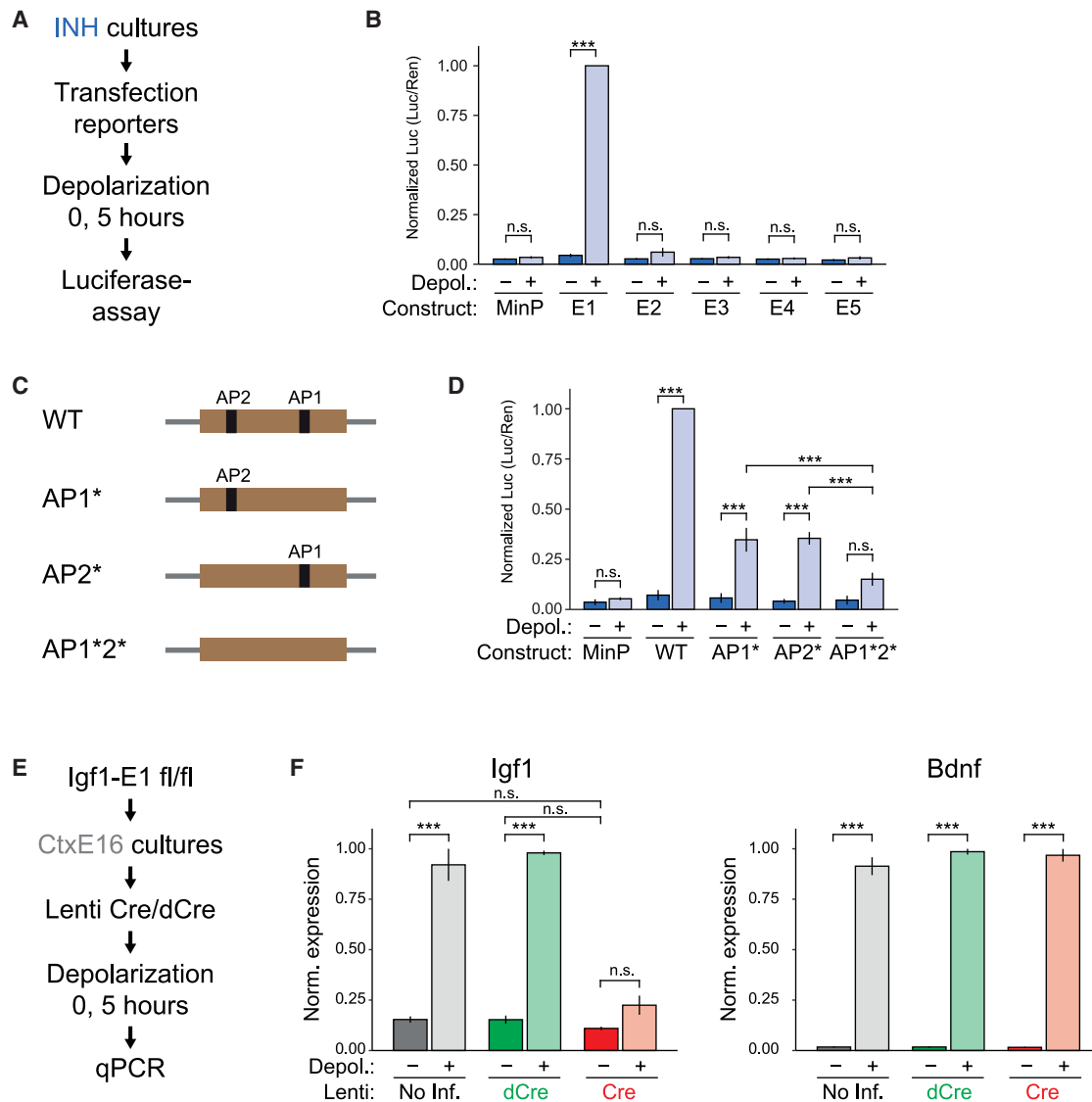
Figure 2. Igf1 enhancer 1 drives the activity-induced transcription of *Igf1* in cultured neurons

(A–D) Luciferase assay to test the enhancer-activity of putative Igf1 enhancers.

(A) Experimental strategy.

(B) Luciferase assay for putative Igf1 enhancers before (−) and after (+) depolarization in inhibitory cultures (n = 3 biological replicates).

(C) Scheme of Igf1 E1 variants lacking one or both AP-1 motifs.

(D) Luciferase activity before (−) or after (+) depolarization with the Igf1 E1 variants (p < 2e−16, two-way ANOVA; n = 4 biological replicates, except for AP1*2 n = 3).

(E and F) Testing whether Igf1 E1 drives activity-dependent *Igf1* transcription in cultured cortical neurons. (E) Experimental strategy. (F) Expression of *Igf1* (left) and *Bdnf* (right) before (−) and after (+) depolarization in control conditions and after Cre-mediated Igf1 E1 cKO in cultured cortical neurons (*Igf1*: p < 6.23e−10, two-way ANOVA; *Bdnf*: p < 2.66e−15; two-way ANOVA, n = 3 biological replicates). (Error bars in all panels represent SEM; p values for all panels indicated by *<0.05, **<0.01, ***<0.001 from Tukey's multiple comparisons).

Using these mice, we then tested whether activity-induced *Igf1* transcription occurs in cultured cortical neurons that lack Igf1 E1. For this, we established cultures of primary cortical neurons from homozygous Igf1-E1 flox mice, transduced the neurons with lentiviral constructs that express either Cre-recombinase or an enzymatically dead version of Cre (dCre), harvested the neurons and extracted RNA before or after depolarization, and then performed reverse transcription followed by quantitative real-time PCR to assess the levels of *Igf1* and *Bdnf* (a well-described late-induced effector gene[13,52]) (Figure 2E). This revealed that cKO of Igf1 E1 abolishes the depolarization-induced increase of *Igf1* but does not affect *Bdnf* induction (Figure 2F). This experiment also revealed that *Igf1* levels in silenced neurons that were not depolarized (i.e., basal, not activity-regulated *Igf1*
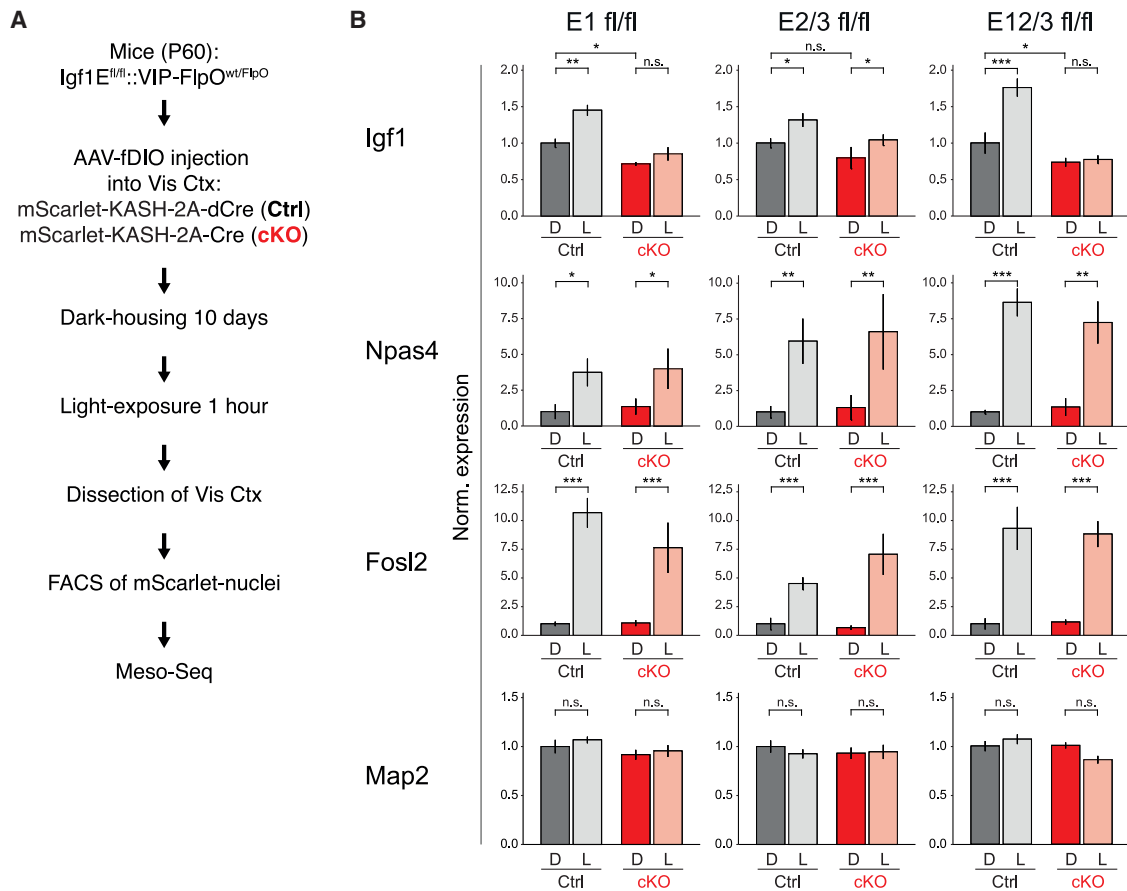
Figure 3. Igf1 enhancers 1 and 2/3 cooperatively drive the sensory-induced transcription of *Igf1* in VIP INs in the adult visual cortex
(A) Experimental strategy for testing whether Igf1 E1 and E2/3 are required for sensory-induced *Igf1* transcription in VIP INs in the visual cortex of adult mice.
(B) Normalized RNA-seq reads upon cKO of the Igf1 enhancers after DH/LE for *Igf1* (FDR[Light] < 7.67e−15, FDR[Light * cKO] < 4.64e−8), *Npas4* (FDR [Light] < 6.77e−7), *Fosl2* (FDR[Light] 1.57e−31) and *Map2* (FDR[Light] > 0.05) (FDR was estimated using Deseq2 likelihood-ratio test; error bars represent SEM; p values of pairwise comparisons indicated by *<0.05, **<0.01, ***<0.001 from Deseq2 Wald-test; n = 4 biological replicates, except for E1 Ctrl D n = 3, E1 Ctrl L n = 5, E1 cKO D n = 5, E12/3 cKO D n = 3).

levels) were not different in E1 cKO and control neurons. Thus, because *Igf1* is expressed in mixed cortical cultures only in inhibitory neurons (Figures S1C–S1E; *Igf1* expression becomes enriched to VIP INs during postnatal development; Figure S1F), we conclude that E1 selectively drives the depolarization-induced upregulation of *Igf1* transcription in cultured inhibitory neurons, but it does not control basal *Igf1* transcription in these neurons.

Igf1 enhancers 1 and 2/3 cooperatively drive the sensory-induced transcription of *Igf1* in VIP INs in the adult visual cortex

Next, we sought to identify the enhancer(s) that drive the sensory-induced transcription of *Igf1* in VIP INs in the adult visual cortex. For this, we devised an intersectional genetic strategy that allowed us to knockout Igf1 E1 and/or E2/3 relatively acutely (i.e., within a few days) and selectively in VIP INs in the adult visual cortex and to test whether this alters sensory-induced *Igf1* transcription in these neurons (Figures S3A–S3D). Such a cell-type-specific and relatively acute genetic approach in the adult

brain is necessary to circumvent potentially confounding factors when knocking out experience-induced genes early during development because KO of such genes can lead to developmental deficits in the wiring and function of neural circuits. Thus, we generated mice that are homozygous for the respective floxed Igf1 enhancer allele and heterozygous for an allele that drives expression of FlpO-recombinase in VIP INs (Vip-IRES-FlpO[53]) (Figure 3A). We injected into the visual cortices of these mice novel adeno-associated viral (AAV) constructs that drive in an Flp-dependent manner the expression of Cre-recombinase (or of dCre as control) and of a nuclear-tethered version of the red-fluorescent protein mScarlet (mScarlet-KASH). We subjected these mice to the well-established DH/LE sensory stimulation protocol,[7,17,27,28,37,54] dissected the visual cortices of these mice, FACS isolated the mScarlet-labeled VIP IN nuclei and analyzed VIP IN-specific gene expression in these nuclei via our recently established Meso-seq protocol[54] (Figure S3E).

This experiment revealed that *Igf1* was significantly sensory induced in control-infected VIP INs in all genotypes, but it also revealed that this induction was attenuated upon cKO of Igf1

E1 (reduction of 58% compared with Ctrl) and completely abolished upon cKO of both enhancers (Figure 3B). The same loss of *Igf1* induction in visual cortex VIP INs lacking Igf1 E1 and E2/3 was observed when we measured *Igf1* levels with an orthogonal approach (single-molecule fluorescence *in situ* hybridization [smFISH]) (Figure S3G). Importantly, Igf1 E1 and E2/3 regulate *Igf1* selectively because (1) the expression of other experience-induced (e.g., *Npas4* and *Fosl2*) and non-regulated (e.g., *Map2*) genes in visual cortex VIP INs remained unaltered upon cKO of these enhancers (Figure 3B) and (2) the few other genes that were mis-regulated in cKO VIP INs are located on different chromosomes than *Igf1* (Figure S3F).

Our experiments also revealed that the levels of *Igf1* in VIP INs lacking Igf1 E1 and E12/3 were slightly reduced in dark-housed mice compared with control-infected VIP INs, thus raising the possibility that these enhancers regulate also the basal (i.e., non-regulated) expression of *Igf1* in VIP INs. Alternatively, because dark-housing does not reduce neuronal activity in visual cortex VIP INs (Figures S4A and S4B) and increases VIP IN excitability (Figures S4I and S4J) it could be that a certain level of activity-induced *Igf1* expression persists in VIP INs even after DH and that this activity-induced *Igf1* expression is lost upon cKO of the Igf1 enhancer(s). Indeed, when we silenced all neuronal activity in the visual cortices of dark-housed mice via the expression of the inward-rectifying K$^+$-channel Kir2.1 (Figures S4C–S4H), we found that *Igf1* levels in visual cortex VIP INs are decreased to a similar degree as in the Igf1 enhancer cKO experiments. We therefore conclude that the *Igf1* levels in visual cortex VIP INs that lack the Igf1 enhancers reflect the actual level of basal (i.e., not activity-driven) *Igf1* expression. Furthermore, because the combined cKO of both Igf1 enhancers has the strongest effect on sensory-induced *Igf1* expression, we conclude that these two enhancers cooperate to selectively drive sensory-induced transcription of *Igf1* in cortical VIP INs.

Igf1 enhancers 1 and 2/3 maintain E/I ratio in VIP INs in the adult visual cortex

VIP IN-derived IGF1 selectively promotes inhibitory inputs onto VIP INs in the developing visual cortex.[27] Thus, having found that Igf1 E1 and E2/3 selectively drive the sensory-induced transcription of *Igf1* in VIP INs in the adult visual cortex, we set out to dissect the cellular-synaptic functions controlled by these enhancers in the adult visual cortex. For this, we took a similar intersectional genetic approach as in our gene expression analyses (Figure 4A): we injected into the visual cortex of adult mice homozygous for the respective floxed Igf1 enhancer(s) and heterozygous for Vip-IRES-FlpO AAV constructs that express in a Flp-dependent manner either Cre-recombinase and EGFP or EGFP alone (as negative control). We housed the mice for 10–14 days under standard conditions, prepared acute visual cortex slices and used whole-cell patch-clamp electrophysiology to record miniature excitatory and inhibitory postsynaptic currents (mEPSCs and mIPSCs, respectively) from EGFP-expressing VIP INs and to calculate the E/I ratio in these neurons. This revealed that cKO of either Igf1 enhancer by itself reduces inhibitory inputs (mIPSCs) onto VIP INs but has no (E2/3) or only subtle (E1) effects on excitatory inputs (mEPSCs)
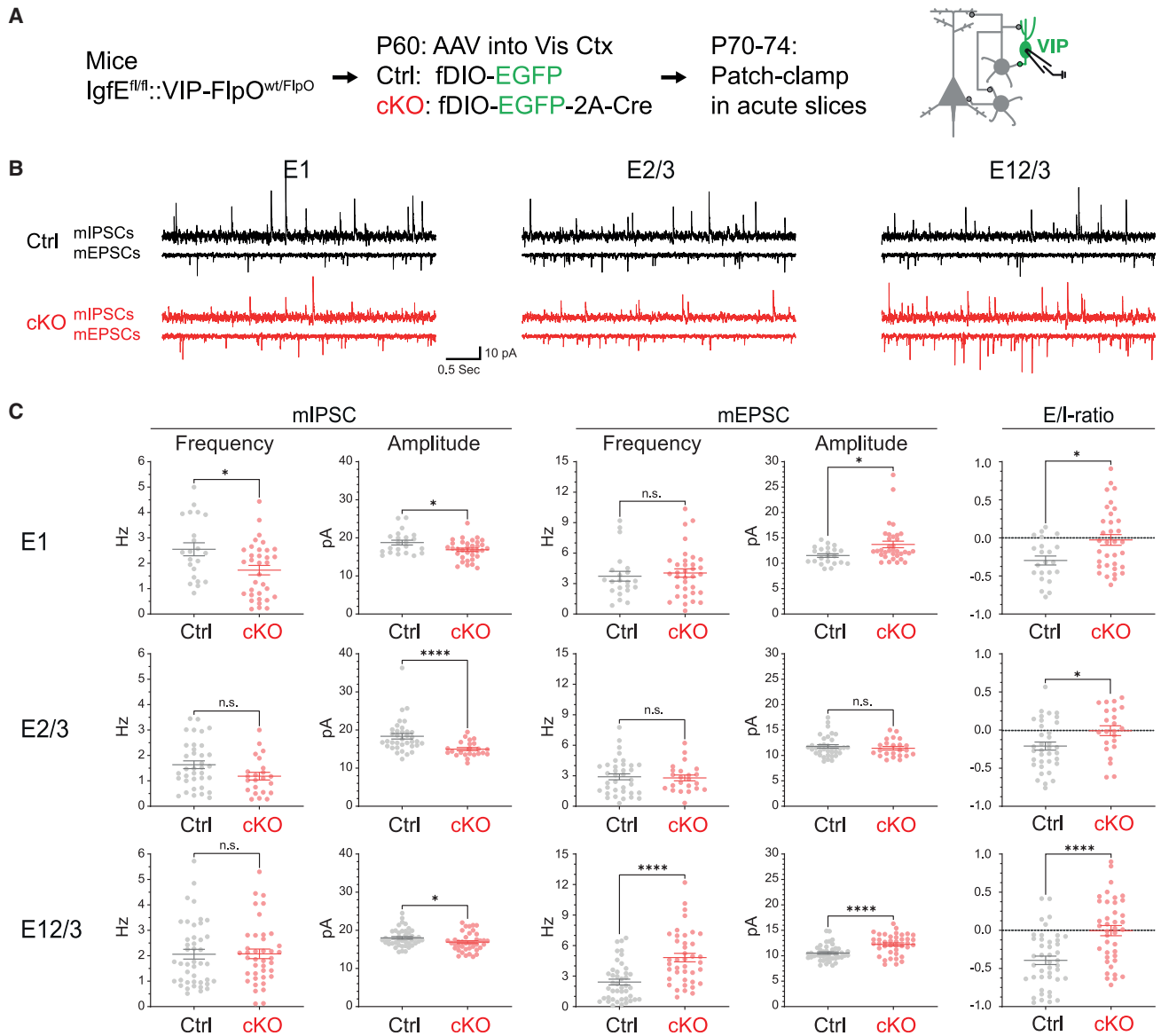
(Figures 4B and 4C) onto VIP INs. In contrast, the cKO of both enhancers causes only a subtle reduction in inhibitory inputs onto VIP INs but a strong increase in their excitatory inputs. Strikingly, however, we find that E/I ratio in VIP INs in all cKO genotypes shifts toward more excitation (Figure 4C). Similar to our previous findings in the developing visual cortex,[27] we did not observe a change in the capacitance of the recorded VIP INs in any of the genotypes (Figure S5A), indicating that the synaptic effects of knocking out Igf1 E1 and E2/3 are not due to changes in the size of VIP INs. Thus, we conclude that sensory-induced transcription of *Igf1* in VIP INs in the adult visual cortex maintains E/I ratio in these neurons by preventing a shift toward more excitation.

Sensory-induced *Igf1* transcription drives sensory-induced plasticity of GABAergic inputs onto VIP INs in the adult visual cortex

A goal of our study was to test whether experience-induced transcription regulates specific forms of experience-dependent synaptic plasticity. Thus, having found that sensory-induced *Igf1* transcription in visual cortex VIP INs maintains E/I ratio in these neurons over time (Figure 4), we next sought to test whether sensory-induced *Igf1* transcription controls acute (i.e., within a few hours) aspects of experience-dependent synaptic plasticity in these neurons.

Because *Igf1* in VIP INs in the adult visual cortex is induced upon DH/LE within a few hours (Figure S1B) and because VIP IN-derived IGF1 selectively promotes inhibitory inputs onto these cells,[27] we hypothesized that LE after DH would lead to an increase in inhibitory inputs onto VIP INs within a few hours and that this increase would require activity-induced transcription of *Igf1*. To test this hypothesis, we used our intersectional genetic approach to knock out all sensory-induced *Igf1* transcription in VIP INs in the adult visual cortex (i.e., cKO of Igf1-E1 and E2/3), dark-housed the injected mice for 2 weeks, then exposed the mice to light for 12 h or left them in the dark for the same amount of time and performed patch-clamp recordings in AAV-infected VIP INs in acute visual cortex slices (Figure 5A). This revealed that LE after DH leads in control-infected VIP INs within hours to a selective increase in mIPSC frequency (Figure 5B) and to a shift in E/I ratio toward more inhibition and that these sensory-induced changes in mIPSC frequency and E/I ratio are abolished in VIP INs lacking activity-induced *Igf1* transcription (i.e., in Igf1 E12/3 cKO VIP INs). Further demonstrating that the synaptic effects exerted by the sensory-induced Igf1 enhancers are sensory dependent, we did not observe in these experiments a change in mEPSCs, mIPSCs, and E/I ratio in Igf1 E12/3 cKO VIP INs in the visual cortex of dark-housed mouse. Finally, we did not observe a change in the capacitance of cKO VIP INs in these acute stimulation experiments (Figure S5B), consistent with the notion that these effects on inhibitory inputs are not due to changes in VIP IN cell size. Thus, taken together, these experiments revealed that activity-induced transcription of *Igf1* in VIP INs in the adult visual cortex selectively drives an acute sensory-induced increase in inhibitory inputs onto these neurons and a concurrent shift in their E/I ratio toward inhibition.

Interestingly, the synaptic effects observed upon cKO of Igf1 E1 and E2/3 in these acute stimulation experiments differ from

A

Mice
IgfE^fl/fl^::VIP-FlpO^wt/FlpO^ → P60: AAV into Vis Ctx
Ctrl: fDIO-EGFP
cKO: fDIO-EGFP-2A-Cre → P70-74:
Patch-clamp
in acute slices

B

C

Figure 4. Lack of sensory-induced Igf1 enhancers shifts E/I ratio in VIP INs toward excitation
(A–C) Whole-cell patch-clamp recordings in acute visual cortex slices to assess the cellular-synaptic effects of Igf1 E1 and/or E2/3 cKO in visual cortex VIP INs of standard-housed mice.
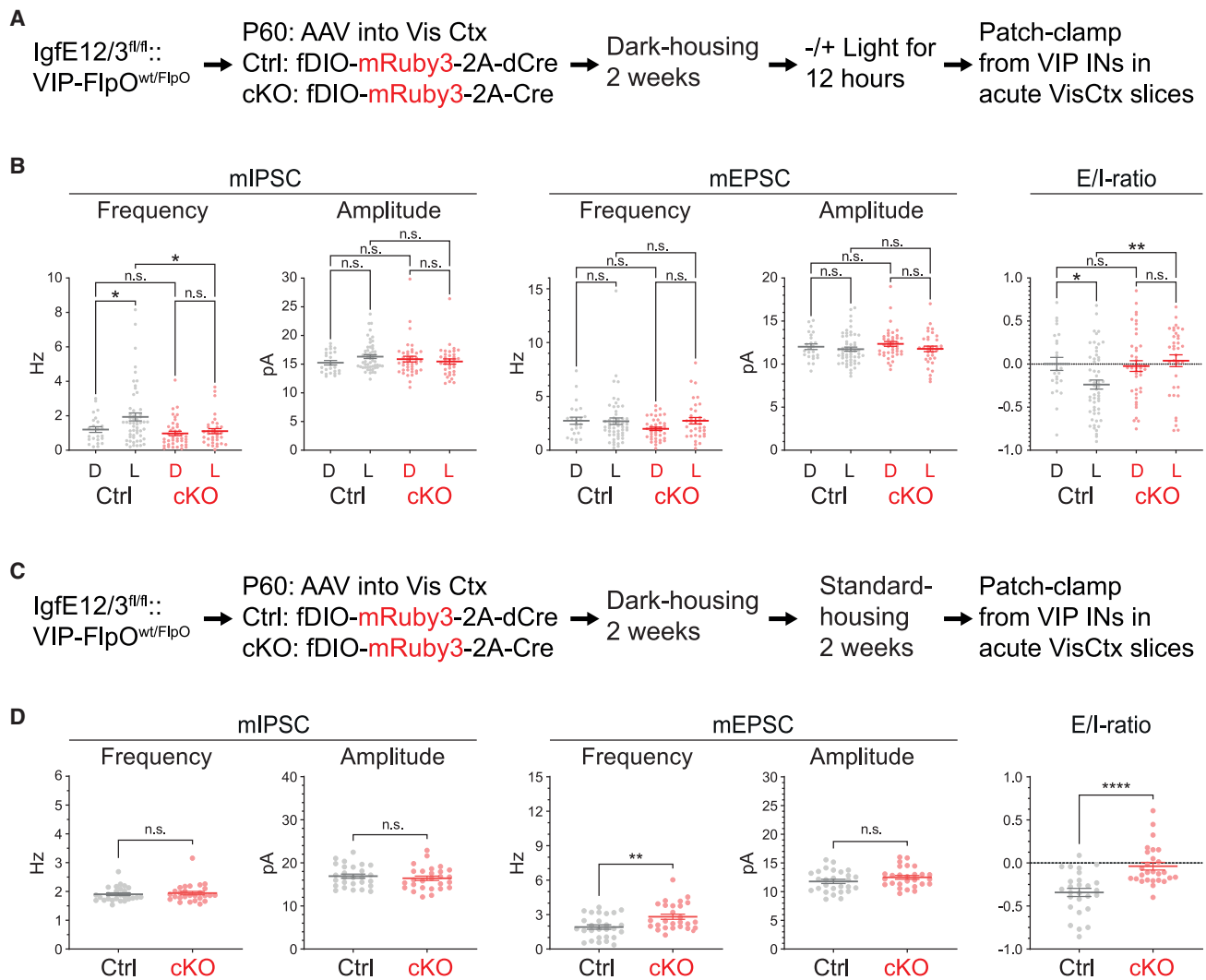(A) Experimental strategy.
(B) Representative traces of miniature excitatory or inhibitory postsynaptic currents (mEPSCs or mIPSCs, respectively) recorded from VIP INs lacking (cKO) or containing (control) the respective Igf1 enhancer(s).
(C) Frequencies and amplitudes of mIPSCs and mEPSCs and E/I ratio upon cKO of the respective Igf1 enhancer(s) (E1: control n = 22, cKO n = 34; E2/3: control n = 36, cKO n = 23; E12/3: control n = 43, cKO n = 40; for descriptive statistics see Table S5). (In all panels: error bars represent SEM, p values of pairwise comparisons indicated by *<0.05, ****<0.0001 from Mann-Whitney test).

those observed when housing the animals under standard conditions for prolonged periods of time upon cKO of both Igf1 enhancers (Figure 4): although E/I ratio is shifted in both experimental settings toward more excitation, in the acute plasticity experiment, this shift is driven by a decrease in inhibitory inputs, whereas in the long-term standard-housing experiments, it is driven by an increase in excitatory inputs. This suggests that the strengthening of inhibitory inputs is the primary function of

sensory-driven *Igf1* transcription in VIP INs and that the increase in excitatory input observed in the long-term experiments is a secondary consequence. Indeed, when we tested this idea directly by knocking out both Igf1 enhancers in visual cortex VIP INs, dark-housing the mice for 2 weeks and then returning them to standard conditions for 2 additional weeks, we found that the shift in E/I ratio is driven again by an increase in excitatory inputs (Figures 5C and 5D), without any changes in the

A

IgfE12/3^{fl/fl}:: VIP-FlpO^{wt/FlpO} → P60: AAV into Vis Ctx
Ctrl: fDIO-mRuby3-2A-dCre
cKO: fDIO-mRuby3-2A-Cre → Dark-housing 2 weeks → -/+ Light for 12 hours → Patch-clamp from VIP INs in acute VisCtx slices

B

C

IgfE12/3^{fl/fl}:: VIP-FlpO^{wt/FlpO} → P60: AAV into Vis Ctx
Ctrl: fDIO-mRuby3-2A-dCre
cKO: fDIO-mRuby3-2A-Cre → Dark-housing 2 weeks → Standard-housing 2 weeks → Patch-clamp from VIP INs in acute VisCtx slices

D

Figure 5. Sensory-induced Igf1 enhancers control sensory-dependent plasticity of inhibitory inputs onto visual cortex VIP INs
Whole-cell patch-clamp recordings in acute cortical slices to assess the effects of Igf1 E1 and E2/3 cKO in visual cortex on mIPSCs and mEPSCs and E/I ratio in VIP INs upon acute dark-housing/light-exposure sensory stimulation (A and B) or upon dark-housing/light-exposure sensory stimulation followed by 2 weeks of standard housing (C and D).
(A and B) Acute sensory stimulation. (A) Experimental strategy. (B) Quantified data (control dark n = 24 cells, control-light n = 55, cKO dark n = 41, cKO light n = 35) (Brown-Forsythe ANOVA test: mIPSC frequency p < 0.0001, mIPSC amplitude p = 0.2808, mEPSC frequency p = 0.1374, mEPSC amplitude p = 0.3470, E/I ratio p = 0.0035; p values of pairwise comparisons indicated by *<0.05, **<0.01 from post hoc Dunnett's T3 multiple comparisons test).
(C and D) Acute sensory stimulation followed by standard housing. (C) Experimental strategy. (D) Quantified data (control n = 27, cKO n = 27) (p values of pairwise comparisons indicated as **<0.01, ****<0.0001 from Mann-Whitney test). (In all data panels error bars represent SEM; for descriptive statistics see Table S5).

cells' capacitance (Figure S5C). Thus, we conclude that the primary cellular-synaptic function of sensory-driven *Igf1* transcription in VIP INs in the adult visual cortex lies in the sensory-dependent promotion of inhibitory inputs onto these neurons. These findings also indicate that the distinct synaptic long-term effect of knocking out only one sensory-induced Igf1 enhancer (Figure 4C) is likely due to the fact that this genetic manipulation reduces experience-induced *Igf1* expression in VIP INs only partially and that the subsequent secondary synaptic effects are less pronounced.

Activity-induced *Igf1* transcription restricts neural activity rates and maintains spatial frequency tuning in the adult visual cortex

Having determined that activity-induced *Igf1* transcription selectively promotes sensory-induced plasticity of inhibitory inputs onto VIP INs in the adult visual cortex, we next sought to assess whether this synaptic plasticity mechanism controls visual cortex function *in vivo* by testing whether the lack of activity-induced *Igf1* transcription in VIP INs alters the activity and response properties of VIP INs in the visual cortex of awake-behaving mice. For
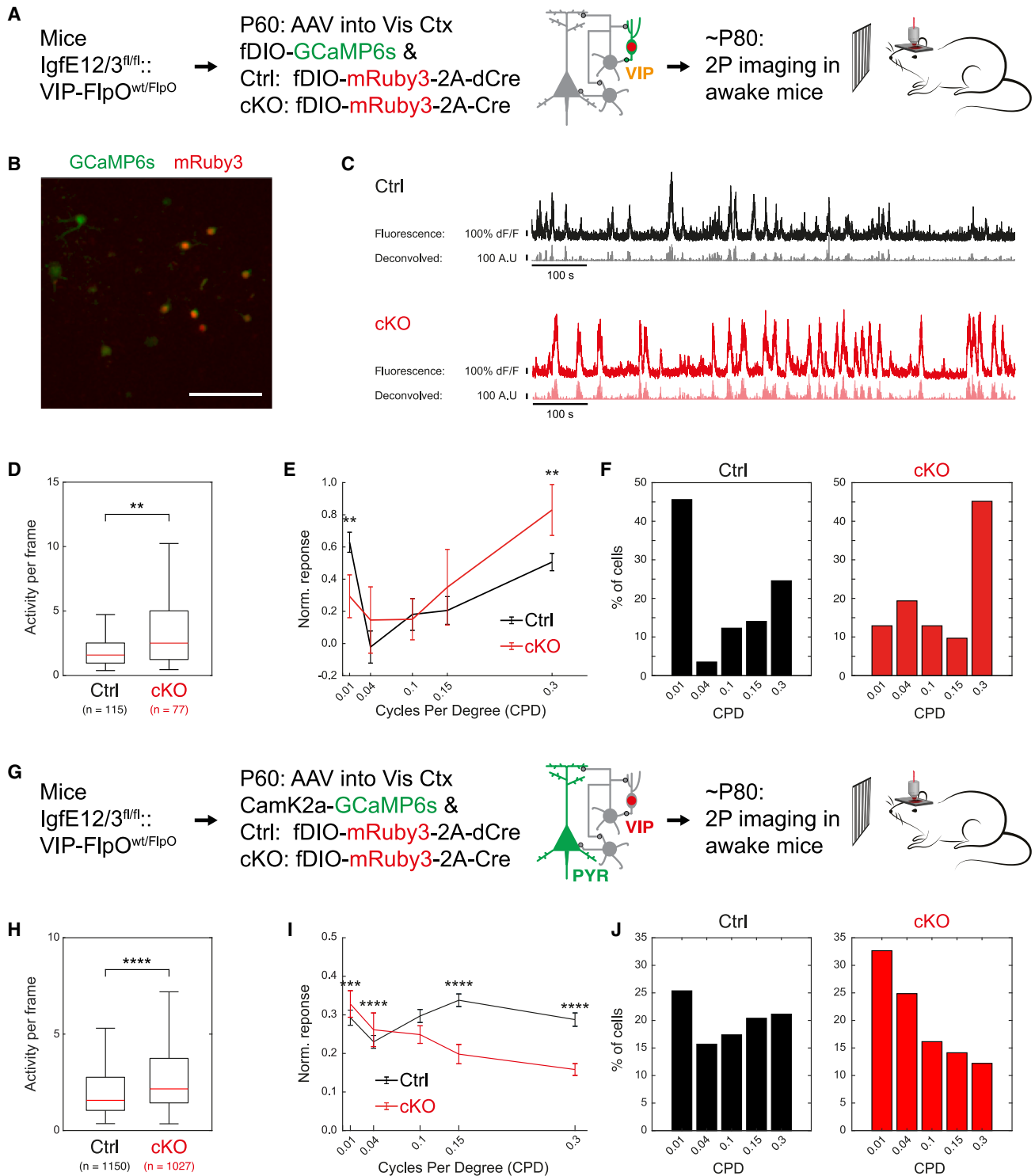
Figure 6. Sensory-induced transcription of *Igf1* in VIP INs maintains neural activity rates in VIP INs in the adult visual cortex and restricts visual acuity

In vivo two-photon GCaMP imaging in the monocular zone of the primary visual cortex (mV1) of adult awake-behaving mice to analyze the effects of knocking out the Igf1 enhancers in VIP INs on the spontaneous activity and visual response properties of visual cortex VIP INs and L2/3 PYR neurons.

(A–F) Effects in VIP INs.

(A) Experimental strategy.

(legend continued on next page)

this, we took a similar intersectional genetic approach as in our electrophysiological experiments and co-injected into the monocular zone (MZ) of the primary visual cortex (V1) of adult mice homozygous for the Igf1-E12/3 flox allele and heterozygous for Vip-IRES-FlpO two Flp-dependent AAV constructs: one construct that drives the expression of the genetically encoded calcium indicator GCaMP6s and another construct that drives the expression of Cre-recombinase (or dCre as control) and of the red-fluorescent protein mRuby3 (Figures S6A and S6B). We then performed two-photon calcium imaging in the visual cortex of these mice while they were awake, head-fixed and placed on a linear treadmill (Figures 6A and 6B). Because the activity and response properties of VIP INs are modulated by behavioral states such as arousal,[32,55] we also performed pupillometry during the imaging sessions as this is a reliable readout for arousal states.[55–58]

Using this setup, we first analyzed the spontaneous activity of cKO and control VIP INs (Figures 6C, 6D, and S6E). This revealed that the spontaneous activity of VIP INs lacking Igf1 E1 and E2/3 was significantly higher than in control-infected VIP INs, which is consistent with our observation that E/I ratio in VIP INs shifts toward more excitation upon cKO of these enhancers (Figure 4C). In turn, this increased spontaneous activity renders Igf1 E12/3 cKO VIP INs more co-active as indicated by the increased cell-to-cell correlation of these neurons (Figure S6C). Notably, these effects do not depend on the animal's arousal state as the arousal-dependent modulation of spontaneous activity in cKO and control VIP INs was nearly identical (Figure S6D). We therefore conclude that sensory-induced transcription of Igf1 in VIP INs, mediated by Igf1 E1 and E2/3, restricts the spontaneous activity of these neurons in the visual cortex in vivo, regardless of the animal's behavioral state.

Next, we asked whether the sensory-induced transcription of Igf1 in VIP INs affects the responses of these neurons to visual stimuli. For this, we focused on spatial frequency tuning because we[27] and Ayzenshtat et al.[59] have found that this visual response property is affected by the activity levels of VIP INs. Consistent with these previous observations, we find that in the absence of sensory-induced Igf1 transcription, spatial frequency tuning in VIP INs increases and shifts toward higher spatial frequencies (Figures 6E and 6F). Thus, spatial frequency tuning in visual cortex VIP INs in awake-behaving mice is restricted by the sensory-induced transcription of Igf1 in VIP INs.

Because VIP INs are powerful regulators of neural activity in cortical circuits[32] and of the response properties of visual cortex neurons,[59,60] we set out to test whether enhancer-mediated sensory-induced Igf1 transcription in VIP INs regulates activity and sensory processing in whole cortical circuits. To this end, we took a similar genetic approach as before but expressed GCaMP in pyramidal (PYR) excitatory neurons instead of in VIP INs and analyzed the activity and response properties of PYR neurons in layer 2/3 (L2/3) of V1 MZ (Figure 6G). This revealed that, consistent with the disinhibitory function of VIP INs,[30,31] the spontaneous activity in L2/3 PYR neurons is elevated when sensory-induced transcription of Igf1 in VIP INs is absent (Figure 6H). Furthermore, these experiments revealed that the spatial frequency tuning of L2/3 PYR neurons is altered in the absence of enhancer-mediated sensory-induced transcription of Igf1 in VIP INs (Figures 6I and 6J). Taken together, these findings demonstrate that the enhancer-mediated sensory-induced transcription of Igf1 in VIP INs restricts neural activity in visual cortex PYR neurons and maintains the spatial frequency tuning of these neurons in awake-behaving mice. We therefore conclude that sensory-induced enhancers, via the transcription of even a single late-induced effector gene, can directly restrict neural activity in vivo and that this, in turn, is necessary for maintaining the response properties of whole neural circuits.

DISCUSSION

Enhancer-mediated activity-induced transcription is thought to promote the plasticity of neural circuits by modulating specific sets of synapses; yet, this fundamental assumption in neuroscience remains untested. Although thousands of putative experience-induced enhancers were identified in multiple types of neurons and brain regions,[7,9,10,36,37,42] the functions of only a few of these enhancers were analyzed experimentally, and these functional analyses focused primarily on the transcriptional regulation of a few well-known activity-regulated genes in cultured neurons (e.g., Fos[42,61] and Bdnf[62]). Thus, no enhancers were identified that selectively drive the activity-induced transcription of specific neuronal genes in the brain in vivo, and the neurobiological functions of specific single experience-regulated enhancers in neural circuits remained unknown. To address this fundamental gap-in-knowledge, we focused on the late-induced synaptic effector gene Igf1 whose transcription is sensory

---

(B) Representative field of view of mV1 VIP INs expressing GCaMP6s and mRuby3-2A-dCre (scale bars, 100 μm).

(C and D) Effects on spontaneous activity in VIP INs. (C) Example traces of fluorescence changes (dF/F) and deconvolved signals in control (upper traces) and cKO (bottom traces) VIP INs. (D) Quantification of spontaneous activity in control and cKO VIP INs (Ctrl: 115 neurons, n = 4 mice, median = 1.58, SEM = 0.25; CKO: 77 neurons, p = 0.0027, median = 2.51, SEM = 0.66; Wilcoxon rank-sum test).

(E and F) Effects on spatial frequency tuning in VIP INs. (E) Normalized population averages of all visually responsive control or cKO VIP INs to drifting gratings at different spatial frequency (cycles per degree [cpd]) (Ctrl: 57 neurons, cKO: 31 neurons). (F) Histogram of the preferred spatial frequency of control (left) and cKO (right) VIP INs.

(G–J) Effects in L2/3 PYR neurons.

(G) Experimental strategy.

(H) Effects on spontaneous activity in L2/3 PYR neurons (Ctrl: 1,150 neurons, median = 1.57, SEM = 0.08; CKO: 1,027 neurons, median = 2.16, SEM = 0.12.

(I and J) Effects on spatial frequency tuning in L2/3 PYR neurons. (I) Normalized population averages of all visually responsive control or cKO L2/3 PYR neurons to drifting gratings at different spatial frequencies (cycles per degree [cpd]) (Ctrl: 1,064 neurons, cKO: 1,090 neurons). (J) Histogram of the preferred spatial frequency of L2/3 PYR neurons next to control (left) and cKO (right) VIP INs.

(Error bars in all data panels represent SEM, p values are indicated as **<0.01, ****<0.0001 from Wilcoxon rank-sum test with four biological replicates [n = 4 mice]).

induced in VIP INs in the adult visual cortex and that promotes inhibitory inputs onto VIP INs in the developing cortex. Our study generated several key findings: (1) the activity-regulated enhancer landscape in cultured mouse cortical inhibitory and excitatory neurons is cell type specific, (2) the *Igf1* locus in VIP INs in the visual cortex of adult mice contains four putative enhancers of which the two major ones—E1 and E2/3—are cell type specific and sensory regulated, (3) in cultured inhibitory neurons, E1 alone drives the activity-induced transcription of *Igf1* but does not control its basal transcription, (4) in VIP INs in the adult visual cortex, E1 and E2/3 drive activity-dependent transcription of *Igf1* partially and cooperate to drive the full activity-induced transcription of *Igf1*, (5) E1 and E2/3, alone and together, control E/I ratio in VIP INs in the adult visual cortex such that in the absence of these enhancers, E/I ratio in VIP INs shifts toward more excitation, (6) the enhancer-mediated activity-induced transcription of *Igf1* in visual cortex VIP INs drives a sensory-induced increase (i.e., plasticity) in inhibitory inputs onto these neurons within a few hours after onset of sensory stimulation, and (7) in VIP INs and in L2/3 PYR neurons in the visual cortex of awake-behaving mice, the enhancer-mediated activity-induced transcription of *Igf1* in VIP INs restricts neural activity and maintains the visual response properties of these neurons. Thus, our study demonstrates that specific single sensory-regulated enhancers and the activity-induced transcription mediated by such enhancers can directly control the processing of sensory information in specific neural circuits *in vivo* in the adult brain.

The results of our cell-type-specific H3K27Ac ChIP-seq experiments in cultured mouse GABAergic neurons are largely consistent with previous studies[10,17]: most of the sites with significantly inducible H3K27Ac peaks are found at putative enhancers, and similar to the activity-regulated transcriptional programs in these cells, the activity-regulated enhancer landscape in these cells is cell type specific. Furthermore, similar to in other types of neurons,[36,37] putative activity-regulated enhancers in GABAergic neurons are enriched for AP-1 binding sites, supporting the idea that the AP-1 complex is part of a ubiquitous transcriptional "responsosome."[47] Future studies will have to identify the molecular mechanisms that determine the cell type specificity of experience-induced enhancers in GABAergic neurons; likely, these mechanisms include molecules that determine cell-type-specific availability of activity-induced enhancers in these cells via, for example, cell-type-specific epigenetic modifications, as well as cell-type-specific molecules (e.g., TFs and lincRNAs) that guide, for example, the AP-1 complex to the available enhancers in each type of neuron.

The stimulus-dependent transcriptional selectivity of the Igf1 enhancers identified by us is remarkable, especially when compared with other activity-regulated enhancers analyzed in their endogenous genomic context: unlike, for example, the activity-induced enhancer found 3 kb upstream of the *Bdnf* TSS, whose knockout leads to reduced levels of *Bdnf* mRNA even in the absence of stimulation,[62] we find that the removal of the Igf1 enhancers does not lower the basal (i.e., non-induced) expression of *Igf1*, neither in cultured GABAergic neurons (Figure 2E) nor in visual cortex VIP INs *in vivo* (as indicated by the

silencing experiments in Figures S4C–S4G). The transcriptional potency of the stimulus-induced Igf1 enhancers is noteworthy as well: unlike in other enhancers where their knockout[61,62] or inhibition[42] leads to reduced but still significant stimulus-induced transcription of their target genes, loss of either E1 in cultured GABAergic neurons or both Igf1 enhancers in visual cortex VIP INs completely abolishes stimulus-induced *Igf1* transcription in these cells. Notably, E1 and E2/3 seem to do so in a cooperative manner: the lack of only E1 leads to a partial reduction in sensory-induced *Igf1* in VIP INs, whereas removing only E2/3 has relatively minor effects, and both enhancers are required for the full sensory-induced upregulation of *Igf1* transcription.

The observation that sensory-induced transcription of *Igf1* in VIP INs in the adult visual cortex promotes inhibitory inputs onto these neurons to maintain E/I ratio in a cell-autonomous manner is one of the central findings of our study. This observation is based on our ability to selectively manipulate only the sensory-induced transcription of *Igf1* in VIP INs in the adult visual cortex without altering its basal transcription: combined with an acute sensory stimulation paradigm, this approach revealed that enhancer-mediated sensory-induced transcription can modulate within a few hours specific sets of inputs onto VIP INs in the adult cortex. This not only supports the notion that VIP INs in the adult cortex are highly plastic[27,33] but also indicates that the function of sensory-induced transcription is beyond "just stocking the shelves," i.e., that the newly transcribed mRNAs are indeed translated into proteins that directly modulate specific aspects of neuronal wiring in response to acute (sensory) stimuli with a time course of several hours. Thus, it will be fascinating to dissect at the single-cell level the temporal and spatial relationships between the newly transcribed mRNAs of a sensory-induced gene, such as *Igf1*, its protein products that might have existed already before stimulus onset, and those protein products that are newly translated off the stimulus-induced mRNAs of this gene.

Our experiments also indicate that sensory-dependent modulation of inhibitory inputs onto VIP INs and maintenance of E/I ratio scale with sensory-induced *Igf1* transcription. Removing each individual enhancer affects transcription less than removing both, and the effects on E/I ratio are more pronounced when both are missing. Along with previous observations,[17,27,49,63,64] this suggests that the primary function of enhancer-mediated experience-induced transcription is to dynamically adjust E/I ratio in each neuron according to the levels of neural activity impinging on it and according to its cell-type-specific setpoint for E/I ratio. Thus, our electrophysiology experiments suggest that sensory-induced enhancers are key components of an experience-dependent genetic mechanism that homeostatically maintains E/I ratio in neurons to thereby ensure the functional stability of neural circuits over time.[65–67] This idea is supported by our imaging experiments in VIP INs and L2/3 PYR neurons in the primary visual cortex of awake-behaving adult mice: we find that the increased excitatory drive in VIP INs caused by the lack of activity-induced *Igf1* transcription in these neurons upon cKO of the Igf1 enhancers leads to VIP INs and L2/3 PYR neurons being more active when no visual stimulation is present (i.e., increased spontaneous activity) and to a change in the spatial frequency tuning

of these neurons. Although the restriction of neural activity in VIP INs and L2/3 PYR neurons by activity-induced *Igf1* transcription in VIP INs is intuitively clear—too much activity in disinhibitory VIP INs is expected to render neighboring excitatory neurons overactive—it is less obvious how changes in spontaneous activity affect response properties, such as spatial frequency tuning. Because the connection between a neuron's spontaneous activity and its tuning properties is still not well understood, the reagents and approaches generated in our study might help to disentangle this relationship in future studies, e.g., via cKO of activity-induced *Igf1* transcription in adult visual cortex VIP INs and longitudinal GCaMP imaging.

In our experiments, we have not directly assessed the role of sensory-induced transcription of *Igf1* in VIP INs in regulating adult visual cortex plasticity, e.g., during learning or in an ocular dominance plasticity (ODP) paradigm. However, considering that (1) VIP INs are disinhibitory[30–32] and disinhibition is a central cellular mechanism for regulating plasticity in adult cortical circuits,[68] (2) VIP INs control the plasticity of adult cortical circuits,[33–35] (3) experience-dependent modulation of inhibitory connectivity determines the extent of plasticity in adult cortical circuits,[69,70] and (4) enhancer-mediated activity-induced transcription of *Igf1* in VIP INs promotes inhibitory inputs onto VIP INs in an experience-dependent manner to maintain proper sensory processing in the adult cortex (this study), it seems likely that Igf1 E1 and E2/3 directly control the plasticity of adult cortical circuits. Thus, a fundamental question is whether sensory-induced *Igf1* transcription via these enhancers indeed promotes cortical plasticity at the circuit level: because knocking out experience-induced genes was repeatedly found to cause deficits in various plasticity paradigms (e.g., during learning,[20,21,25] in addiction,[22,23] and visual cortex plasticity[27,71,72]), experience-induced transcription is generally thought to promote neural circuit plasticity. However, considering the apparent homeostatic function of sensory-induced *Igf1* transcription in VIP INs and of other sensory-regulated genes in other types of cortical neurons,[3,4] this view probably has to be revised: it seems that—at least in neocortical circuits—the experience-induced transcription of many genes restricts rather than promotes circuit plasticity. The purpose of such a plasticity-restricting function of experience-induced transcription remains to be determined, but one attractive idea is that experience-induced transcription homeostatically counteracts other forms of cellular plasticity (e.g., Hebbian plasticity) to thereby convey functional stability to cortical circuits over time.

Even subtle mutations in TFBSs in experience-induced enhancers (e.g., deletion of the AP-1 sites in E1; see Figure 2) can impair the ability of such enhancers to drive experience-induced gene transcription; thus, our findings also suggest that naturally occurring sequence variations in experience-regulated enhancers in the human genome—e.g., single-nucleotide polymorphisms (SNPs) or mutations associated with neurological or neuropsychiatric disorders—might affect an individual's ability to perceive and learn from sensory information. Although future studies will have to elucidate the specific short- and long-term effects of such mutations at the level of cells, synapses, and circuits, our current study provides a conceptual roadmap for such future investigations.

STAR★METHODS

Detailed methods are provided in the online version of this paper and include the following:

- KEY RESOURCES TABLE
- RESOURCE AVAILABILITY
  - Lead contact
  - Materials availability
  - Data and code availability
- EXPERIMENTAL MODEL AND SUBJECT DETAILS
  - Animals and dark-housing/light-exposure (DH/LE) sensory stimulation paradigm
- METHOD DETAILS
  - Neuronal cell cultures
  - H3K27Ac ChIP-seq from cultured inhibitory and excitatory neurons
  - Cloning of DNA constructs
  - Luciferase assay
  - Generation of cKO animals
  - Lentiviral production
  - AAV production
  - Stereotactic intra-cortical injections of AAV constructs
  - Meso-seq
  - RNAscope fluorescence in situ hybridization (FISH)
  - Immunohistochemistry
  - Patch-clamp electrophysiology in acute visual cortex slices
  - *In vivo* 2-photon imaging
  - Data analyses

AUTHOR CONTRIBUTIONS

I.S. initiated and conceived this project. O.R. generated the floxed enhancer mice and performed all the experiments and analyses in Figures 1, 2, 3, S1–S3, S4C, and S4F–S4H (with the exception of the H3K27Ac ChIP-seq experiments in inhibitory or excitatory neuronal cultures, which were done by H.W.G. and I.S.). E.Z. performed all the experiments and analyses in Figures 4, 5, S4D,

REFERENCES

1. Citri, A., and Malenka, R.C. (2008). Synaptic plasticity: multiple forms, functions, and mechanisms. Neuropsychopharmacology 33, 18–41.

2. Diering, G.H., and Huganir, R.L. (2018). The AMPA receptor code of synaptic plasticity. Neuron 100, 314–329.

3. Yap, E.-L., and Greenberg, M.E. (2018). Activity-regulated transcription: bridging the gap between neural activity and behavior. Neuron 100, 330–348.

4. Gray, J.M., and Spiegel, I. (2019). Cell-type-specific programs for activity-regulated gene expression. Curr. Opin. Neurobiol. 56, 33–39.

5. Leslie, J.H., and Nedivi, E. (2011). Activity-regulated genes as mediators of neural circuit plasticity. Prog. Neurobiol. 94, 223–237.

6. Alberini, C.M. (2009). Transcription factors in long-term memory and synaptic plasticity. Physiol. Rev. 89, 121–145.

7. Stroud, H., Yang, M.G., Tsitohay, Y.N., Davis, C.P., Sherman, M.A., Hrvatin, S., Ling, E., and Greenberg, M.E. (2020). An activity-mediated transition in transcription in early postnatal neurons. Neuron 107, 874–890.e8.

8. Fernandez-Albert, J., Lipinski, M., Lopez-Cascales, M.T., Rowley, M.J., Martin-Gonzalez, A.M., Del Blanco, B., Corces, V.G., and Barco, A. (2019). Immediate and deferred epigenomic signatures of in vivo neuronal activation in mouse hippocampus. Nat. Neurosci. 22, 1718–1730.

9. Su, Y., Shin, J., Zhong, C., Wang, S., Roychowdhury, P., Lim, J., Kim, D., Ming, G.L., and Song, H. (2017). Neuronal activity modifies the chromatin accessibility landscape in the adult brain. Nat. Neurosci. 20, 476–483.

10. Boulting, G.L., Durresi, E., Ataman, B., Sherman, M.A., Mei, K., Harmin, D.A., Carter, A.C., Hochbaum, D.R., Granger, A.J., Engreitz, J.M., et al. (2021). Activity-dependent regulome of human GABAergic neurons reveals new patterns of gene regulation and neurological disease heritability. Nat. Neurosci. 24, 437–448.

11. Li, M., Santpere, G., Imamura Kawasawa, Y., Evgrafov, O.V., Gulden, F.O., Pochareddy, S., Sunkin, S.M., Li, Z., Shin, Y., Zhu, Y., et al. (2018). Integrative functional genomic analysis of human brain development and neuropsychiatric risks. Science 362, eaat7615. https://doi.org/10.1126/science.aat7615.

12. Reilly, S.K., Yin, J., Ayoub, A.E., Emera, D., Leng, J., Cotney, J., Sarro, R., Rakic, P., and Noonan, J.P. (2015). Evolutionary genomics. Evolutionary changes in promoter and enhancer activity during human corticogenesis. Science 347, 1155–1159.

13. Hong, E.J., McCord, A.E., and Greenberg, M.E. (2008). A biological function for the neuronal activity-dependent component of BDNF transcription in the development of cortical inhibition. Neuron 60, 610–624.

14. Sakata, K., Woo, N.H., Martinowich, K., Greene, J.S., Schloesser, R.J., Shen, L., and Lu, B. (2009). Critical role of promoter IV-driven BDNF transcription in GABAergic transmission and synaptic plasticity in the prefrontal cortex. Proc. Natl. Acad. Sci. USA 106, 5942–5947.

15. Nedivi, E., Wu, G.Y., and Cline, H.T. (1998). Promotion of dendritic growth by CPG15, an activity-induced signaling molecule. Science 281, 1863–1866.

16. Chang, M.C., Park, J.M., Pelkey, K.A., Grabenstatter, H.L., Xu, D., Linden, D.J., Sutula, T.P., McBain, C.J., and Worley, P.F. (2010). Narp regulates homeostatic scaling of excitatory synapses on parvalbumin-expressing interneurons. Nat. Neurosci. 13, 1090–1097.

17. Spiegel, I., Mardinly, A.R., Gabel, H.W., Bazinet, J.E., Couch, C.H., Tzeng, C.P., Harmin, D.A., and Greenberg, M.E. (2014). Npas4 regulates excitatory-inhibitory balance within neural circuits through cell-type-specific gene programs. Cell 157, 1216–1229.

18. Favuzzi, E., Deogracias, R., Marques-Smith, A., Maeso, P., Jezequel, J., Exposito-Alonso, D., Balia, M., Kroon, T., Hinojosa, A.J., F Maraver, E., et al. (2019). Distinct molecular programs regulate synapse specificity in cortical inhibitory circuits. Science 363, 413–417.

19. Brigidi, G.S., Hayes, M.G.B., Delos Santos, N.P., Hartzell, A.L., Texari, L., Lin, P.A., Bartlett, A., Ecker, J.R., Benner, C., Heinz, S., et al. (2019). Genomic decoding of neuronal depolarization by stimulus-specific NPAS4 heterodimers. Cell 179, 373–391.e27.

20. Ramamoorthi, K., Fropf, R., Belfort, G.M., Fitzmaurice, H.L., McKinney, R.M., Neve, R.L., Otto, T., and Lin, Y. (2011). Npas4 regulates a transcriptional program in CA3 required for contextual memory formation. Science 334, 1669–1675.

21. Czerniawski, J., Ree, F., Chia, C., Ramamoorthi, K., Kumata, Y., and Otto, T.A. (2011). The importance of having Arc: expression of the immediate-early gene Arc is required for hippocampus-dependent fear conditioning and blocked by NMDA receptor antagonism. J. Neurosci. 31, 11200–11207.

22. Carlezon, W.A., Jr., Thome, J., Olson, V.G., Lane-Ladd, S.B., Brodkin, E.S., Hiroi, N., Duman, R.S., Neve, R.L., and Nestler, E.J. (1998). Regulation of cocaine reward by CREB. Science 282, 2272–2275.

23. Taniguchi, M., Carreira, M.B., Cooper, Y.A., Bobadilla, A.-C., Heinsbroek, J.A., Koike, N., Larson, E.B., Balmuth, E.A., Hughes, B.W., Penrod, R.D., et al. (2017). HDAC5 and its target gene, Npas4, function in the nucleus accumbens to regulate cocaine-conditioned behaviors. Neuron 96, 130–144.e6.

24. Egan, M.F., Kojima, M., Callicott, J.H., Goldberg, T.E., Kolachana, B.S., Bertolino, A., Zaitsev, E., Gold, B., Goldman, D., Dean, M., et al. (2003). The BDNF val66met polymorphism affects activity-dependent secretion of BDNF and human memory and hippocampal function. Cell 112, 257–269.

25. Diering, G.H., Nirujogi, R.S., Roth, R.H., Worley, P.F., Pandey, A., and Huganir, R.L. (2017). Homer1a drives homeostatic scaling-down of excitatory synapses during sleep. Science 355, 511–515.

26. Spiegel, I. (2021). Experience-regulated molecular mechanisms in cortical GABAergic interneurons: from cellular functions to control over circuit plasticity. Curr. Opin. Neurobiol. 67, 145–154.

27. Mardinly, A.R., Spiegel, I., Patrizi, A., Centofante, E., Bazinet, J.E., Tzeng, C.P., Mandel-Brehm, C., Harmin, D.A., Adesnik, H., Fagiolini, M., et al. (2016). Sensory experience regulates cortical inhibition by inducing IGF1 in VIP neurons. Nature 531, 371–375.

28. Hrvatin, S., Hochbaum, D.R., Nagy, M.A., Cicconet, M., Robertson, K., Cheadle, L., Zilionis, R., Ratner, A., Borges-Monroy, R., Klein, A.M., et al. (2018). Single-cell analysis of experience-dependent transcriptomic states in the mouse visual cortex. Nat. Neurosci. 21, 120–129.

29. Hong, S.J., Li, H., Becker, K.G., Dawson, V.L., and Dawson, T.M. (2004). Identification and analysis of plasticity-induced late-response genes. Proc. Natl. Acad. Sci. USA 101, 2145–2150.

30. Lee, S., Kruglikov, I., Huang, Z.J., Fishell, G., and Rudy, B. (2013). A disinhibitory circuit mediates motor integration in the somatosensory cortex. Nat. Neurosci. 16, 1662–1670.

31. Pi, H.-J., Hangya, B., Kvitsiani, D., Sanders, J.I., Huang, Z.J., and Kepecs, A. (2013). Cortical interneurons that specialize in disinhibitory control. Nature *503*, 521–524.

32. Fu, Y., Tucciarone, J.M., Espinosa, J.S., Sheng, N., Darcy, D.P., Nicoll, R.A., Huang, Z.J., and Stryker, M.P. (2014). A cortical circuit for gain control by behavioral state. Cell *156*, 1139–1152.

33. Fu, Y., Kaneko, M., Tang, Y., Alvarez-Buylla, A., and Stryker, M.P. (2015). A cortical disinhibitory circuit for enhancing adult plasticity. eLife *4*, e05558.

34. Melzer, S., Newmark, E.R., Mizuno, G.O., Hyun, M., Philson, A.C., Quiroli, E., Righetti, B., Gregory, M.R., Huang, K.W., Levasseur, J., et al. (2021). Bombesin-like peptide recruits disinhibitory cortical circuits and enhances fear memories. Cell *184*, 5622–5634.e25.

35. Williams, L.E., and Holtmaat, A. (2019). Higher-order thalamocortical inputs gate synaptic long-term potentiation via disinhibition. Neuron *101*, 91–102.e4.

36. Kim, T.-K., Hemberg, M., Gray, J.M., Costa, A.M., Bear, D.M., Wu, J., Harmin, D.A., Laptewicz, M., Barbara-Haley, K., Kuersten, S., et al. (2010). Widespread transcription at neuronal activity-regulated enhancers. Nature *465*, 182–187.

37. Malik, A.N., Vierbuchen, T., Hemberg, M., Rubin, A.A., Ling, E., Couch, C.H., Stroud, H., Spiegel, I., Farh, K.K.-H., Harmin, D.A., et al. (2014). Genome-wide identification and characterization of functional neuronal activity-dependent enhancers. Nat. Neurosci. *17*, 1330–1339.

38. Mo, A., Mukamel, E.A., Davis, F.P., Luo, C., Henry, G.L., Picard, S., Urich, M.A., Nery, J.R., Sejnowski, T.J., Lister, R., et al. (2015). Epigenomic signatures of neuronal diversity in the mammalian brain. Neuron *86*, 1369–1384.

39. Stroud, H., Su, S.C., Hrvatin, S., Greben, A.W., Renthal, W., Boxer, L.D., Nagy, M.A., Hochbaum, D.R., Kinde, B., Gabel, H.W., et al. (2017). Early-life gene expression in neurons modulates lasting epigenetic states. Cell *171*, 1151–1164.e16.

40. Creyghton, M.P., Cheng, A.W., Welstead, G.G., Kooistra, T., Carey, B.W., Steine, E.J., Hanna, J., Lodato, M.A., Frampton, G.M., Sharp, P.A., et al. (2010). Histone H3K27ac separates active from poised enhancers and predicts developmental state. Proc. Natl. Acad. Sci. USA *107*, 21931–21936.

41. Rada-Iglesias, A., Bajpai, R., Swigut, T., Brugmann, S.A., Flynn, R.A., and Wysocka, J. (2011). A unique chromatin signature uncovers early developmental enhancers in humans. Nature *470*, 279–283.

42. Carullo, N.V.N., Phillips, R.A., iii Simon, R.C., Soto, S.A.R., Hinds, J.E., Salisbury, A.J., Revanna, J.S., Bunner, K.D., Ianov, L., Sultan, F.A., et al. (2020). Enhancer RNAs predict enhancer-gene regulatory links and are critical for enhancer function in neuronal systems. Nucleic Acids Res. *48*, 9550–9570.

43. Visel, A., Blow, M.J., Li, Z., Zhang, T., Akiyama, J.A., Holt, A., Plajzer-Frick, I., Shoukry, M., Wright, C., Chen, F., et al. (2009). ChIP-seq accurately predicts tissue-specific activity of enhancers. Nature *457*, 854–858.

44. Preissl, S., Fang, R., Huang, H., Zhao, Y., Raviram, R., Gorkin, D.U., Zhang, Y., Sos, B.C., Afzal, V., Dickel, D.E., et al. (2018). Single-nucleus analysis of accessible chromatin in developing mouse forebrain reveals cell-type-specific transcriptional regulation. Nat. Neurosci. *21*, 432–439.

45. Blankvoort, S., Witter, M.P., Noonan, J., Cotney, J., and Kentros, C. (2018). Marked diversity of unique cortical enhancers enables neuron-specific tools by enhancer-driven gene expression. Curr. Biol. *28*, 2103–2114.e5.

46. Halazonetis, T.D., Georgopoulos, K., Greenberg, M.E., and Leder, P. (1988). C-Jun dimerizes with itself and with c-Fos, forming complexes of different DNA binding affinities. Cell *55*, 917–924.

47. Vierbuchen, T., Ling, E., Cowley, C.J., Couch, C.H., Wang, X., Harmin, D.A., Roberts, C.W.M., and Greenberg, M.E. (2017). AP-1 transcription factors and the BAF complex mediate signal-dependent enhancer selection. Mol. Cell *68*, 1067–1082.e12.

48. Eferl, R., and Wagner, E.F. (2003). AP-1: a double-edged sword in tumorigenesis. Nat. Rev. Cancer *3*, 859–868.

49. Yap, E.-L., Pettit, N.L., Davis, C.P., Nagy, M.A., Harmin, D.A., Golden, E., Dagliyan, O., Lin, C., Rudolph, S., Sharma, N., et al. (2021). Bidirectional perisomatic inhibitory plasticity of a Fos neuronal network. Nature *590*, 115–121.

50. Whyte, W.A., Orlando, D.A., Hnisz, D., Abraham, B.J., Lin, C.Y., Kagey, M.H., Rahl, P.B., Lee, T.I., and Young, R.A. (2013). Master transcription factors and mediator establish super-enhancers at key cell identity genes. Cell *153*, 307–319.

51. Long, H.K., Prescott, S.L., and Wysocka, J. (2016). Ever-changing landscapes: transcriptional enhancers in development and evolution. Cell *167*, 1170–1187.

52. Castrén, E., Zafra, F., Thoenen, H., and Lindholm, D. (1992). Light regulates expression of brain-derived neurotrophic factor mRNA in rat visual cortex. Proc. Natl. Acad. Sci. USA *89*, 9444–9448.

53. He, M., Tucciarone, J., Lee, S., Nigro, M.J., Kim, Y., Levine, J.M., Kelly, S.M., Krugikov, I., Wu, P., Chen, Y., et al. (2016). Strategies and tools for combinatorial targeting of GABAergic neurons in mouse cerebral cortex. Neuron *92*, 555.

54. Apelblat, D., Roethler, O., Bitan, L., Keren-Shaul, H., and Spiegel, I. (2022). Meso-seq for in-depth transcriptomics in ultra-low amounts of FACS-purified neuronal nuclei. Cell Rep. Methods *2*, 100259.

55. Reimer, J., Froudarakis, E., Cadwell, C.R., Yatsenko, D., Denfield, G.H., and Tolias, A.S. (2014). Pupil fluctuations track fast switching of cortical states during quiet wakefulness. Neuron *84*, 355–362.

56. McGinley, M.J., David, S.V., and McCormick, D.A. (2015). Cortical membrane potential signature of optimal states for sensory signal detection. Neuron *87*, 179–192.

57. Vinck, M., Batista-Brito, R., Knoblich, U., and Cardin, J.A. (2015). Arousal and locomotion make distinct contributions to cortical activity patterns and visual encoding. Neuron *86*, 740–754.

58. Cohen-Kashi Malina, K., Tsivourakis, E., Kushinsky, D., Apelblat, D., Shtiglitz, S., Zohar, E., Sokoletsky, M., Tasaka, G.-I., Mizrahi, A., Lampl, I., et al. (2021). NDNF interneurons in layer 1 gain-modulate whole cortical columns according to an animal's behavioral state. Neuron *109*, 2150–2164.e5.

59. Ayzenshtat, I., Karnani, M.M., Jackson, J., and Yuste, R. (2016). Cortical control of spatial resolution by VIP+ interneurons. J. Neurosci. *36*, 11498–11509.

60. Veit, J., Handy, G., Mossing, D.P., Doiron, B., and Adesnik, H. (2023). Cortical VIP neurons locally control the gain but globally control the coherence of gamma band rhythms. Neuron *111*, 405–417.e5.

61. Joo, J.-Y., Schaukowitch, K., Farbiak, L., Kilaru, G., and Kim, T.-K. (2016). Stimulus-specific combinatorial functionality of neuronal c-fos enhancers. Nat. Neurosci. *19*, 75–83.

62. Tuvikene, J., Esvald, E.-E., Rähni, A., Uustalu, K., Zhuravskaya, A., Avarlaid, A., Makeyev, E.V., and Timmusk, T. (2021). Intronic enhancer region governs transcript-specific BDNF expression in rodent neurons. eLife *10*, e65161. https://doi.org/10.7554/eLife.65161.

63. Lin, Y., Bloodgood, B.L., Hauser, J.L., Lapan, A.D., Koon, A.C., Kim, T.K., Hu, L.S., Malik, A.N., and Greenberg, M.E. (2008). Activity-dependent regulation of inhibitory synapse development by Npas4. Nature *455*, 1198–1204.

64. Xue, M., Atallah, B.V., and Scanziani, M. (2014). Equalizing excitation-inhibition ratios across visual cortical neurons. Nature *511*, 596–600.

65. Abbott, L.F., and Nelson, S.B. (2000). Synaptic plasticity: taming the beast. Nat. Neurosci. *3*, 1178–1183.

66. Turrigiano, G.G. (2017). The dialectic of Hebb and homeostasis. Philos. Trans. R. Soc. Lond. B Biol. Sci. *372*. https://doi.org/10.1098/rstb.2016.0258.

67. Vogels, T.P., Sprekeler, H., Zenke, F., Clopath, C., and Gerstner, W. (2011). Inhibitory plasticity balances excitation and inhibition in sensory pathways and memory networks. Science *334*, 1569–1573.

68. Letzkus, J.J., Wolff, S.B.E., and Lüthi, A. (2015). Disinhibition, a circuit mechanism for associative learning and memory. Neuron *88*, 264–276.

69. Mongillo, G., Rumpel, S., and Loewenstein, Y. (2018). Inhibitory connectivity defines the realm of excitatory plasticity. Nat. Neurosci. *21*, 1463–1470.

70. Wilmes, K.A., and Clopath, C. (2019). Inhibitory microcircuits for top-down plasticity of sensory representations. Nat. Commun. *10*, 5055.

71. McCurry, C.L., Shepherd, J.D., Tropea, D., Wang, K.H., Bear, M.F., and Sur, M. (2010). Loss of Arc renders the visual cortex impervious to the effects of sensory experience or deprivation. Nat. Neurosci. *13*, 450–457.

72. Maya-Vetencourt, J.F., Tiraboschi, E., Greco, D., Restani, L., Cerri, C., Auvinen, P., Maffei, L., and Castrén, E. (2012). Experience-dependent expression of NPAS4 regulates plasticity in adult visual cortex. J. Physiol. *590*, 4777–4787.

73. Challis, R.C., Ravindra Kumar, S., Chan, K.Y., Challis, C., Beadle, K., Jang, M.J., Kim, H.M., Rajendran, P.S., Tompkins, J.D., Shivkumar, K., et al. (2019). Systemic AAV vectors for widespread and targeted gene delivery in rodents. Nat. Protoc. *14*, 379–414.

74. Dani, V.S., Chang, Q., Maffei, A., Turrigiano, G.G., Jaenisch, R., and Nelson, S.B. (2005). Reduced cortical activity due to a shift in the balance between excitation and inhibition in a mouse model of Rett syndrome. Proc. Natl. Acad. Sci. USA *102*, 12560–12565.

75. Gouwens, N.W., Sorensen, S.A., Berg, J., Lee, C., Jarsky, T., Ting, J., Sunkin, S.M., Feng, D., Anastassiou, C.A., Barkan, E., et al. (2019). Classification of electrophysiological and morphological neuron types in the mouse visual cortex. Nat. Neurosci. *22*, 1182–1195.

76. Gordon, J.A., and Stryker, M.P. (1996). Experience-dependent plasticity of binocular responses in the primary visual cortex of the mouse. J. Neurosci. *16*, 3274–3286.

77. Martin, M. (2011). Cutadapt removes adapter sequences from high-throughput sequencing reads. EMBnet.journal *17*, 10–12.

78. Langmead, B., and Salzberg, S.L. (2012). Fast gapped-read alignment with Bowtie 2. Nat. Methods *9*, 357–359.

79. Li, H., Handsaker, B., Wysoker, A., Fennell, T., Ruan, J., Homer, N., Marth, G., Abecasis, G., and Durbin, R.; 1000 Genome Project Data Processing Subgroup (2009). The Sequence Alignment/Map format and SAMtools. Bioinformatics *25*, 2078–2079.

80. Li, H. (2011). A statistical framework for SNP calling, mutation discovery, association mapping and population genetical parameter estimation from sequencing data. Bioinformatics *27*, 2987–2993.

81. Feng, J., Liu, T., Qin, B., Zhang, Y., and Liu, X.S. (2012). Identifying ChIP-seq enrichment using MACS. Nat. Protoc. *7*, 1728–1740.

82. Ross-Innes, C.S., Stark, R., Teschendorff, A.E., Holmes, K.A., Ali, H.R., Dunning, M.J., Brown, G.D., Gojis, O., Ellis, I.O., Green, A.R., et al. (2012). Differential oestrogen receptor binding is associated with clinical outcome in breast cancer. Nature *481*, 389–393.

83. Yu, G., Wang, L.-G., and He, Q.-Y. (2015). ChIPseeker: an R/Bioconductor package for ChIP peak annotation, comparison and visualization. Bioinformatics *31*, 2382–2383.

84. Heinz, S., Benner, C., Spann, N., Bertolino, E., Lin, Y.C., Laslo, P., Cheng, J.X., Murre, C., Singh, H., and Glass, C.K. (2010). Simple combinations of lineage-determining transcription factors prime cis-regulatory elements required for macrophage and B cell identities. Mol. Cell *38*, 576–589.

85. Dobin, A., Davis, C.A., Schlesinger, F., Drenkow, J., Zaleski, C., Jha, S., Batut, P., Chaisson, M., and Gingeras, T.R. (2013). STAR: ultrafast universal RNA-seq aligner. Bioinformatics *29*, 15–21.

86. Love, M.I., Huber, W., and Anders, S. (2014). Moderated estimation of fold change and dispersion for RNA-seq data with DESeq2. Genome Biol. *15*, 550.

87. Pachitariu, M., Stringer, C., Dipoppa, M., Schröder, S., Federico Rossi, L., Dalgleish, H., Carandini, M., and Harris, K.D. (2017). Suite2p: beyond 10,000 neurons with standard two-photon microscopy. https://doi.org/10.1101/061507.

STAR★METHODS

KEY RESOURCES TABLE

REAGENT or RESOURCE	SOURCE	IDENTIFIER
Antibodies		
Rabbit-anti-H3K27Ac	Abcam	Cat# ab4729; RRID: AB_2118291
Rabbit-anti-VIP	ImmunoStar	Cat# 20077; RRID: AB_572270
Goat-anti-rabbit Alexa 488	Molecular Probes	Cat# A-11039; RRID: AB_142924
Bacterial and virus strains		
pLenti-hUbc-Cre-GFP	This paper	N/A
pLenti-hUbc-dCre-GFP	This paper	N/A
AAV-Syn1-fDIO-mScarlet-KASH-2a-Cre (pDJ)	This paper	N/A
AAV-Syn1-fDIO-mScarlet-KASH-2a-dCre (pDJ)	This paper	N/A
AAV-Ef1a-fDIO-eGFP-2A-Cre-WPRE (pDJ)	This paper	N/A
AAV-hSyn-Kir2.1WT-2A-mScarlet-KASH	This paper	N/A
AAV-hSyn-Kir2.1Mut-2A-mScarlet-KASH	This paper	N/A
AAV-Ef1a-fDIO-eGFP-WPRE (pDJ)	This paper	N/A
AAV-Ef1a-fDIO-mRuby3-2A-Cre (pDJ)	This paper	N/A
AAV-Ef1a-fDIO-mRuby3-2A-dCre (pDJ)	This paper	N/A
AAV-Ef1a-fDIO-GCaMP6s (pDJ)	Gift from Rylan Larsen	RRID: Addgene_105714
AAV-CamK2a-GCaMP6s-WPRE-SV40 (AAV9)	Gift from Dr. J. M. Wilson	RRID: Addgene_107790
Chemicals, peptides, and recombinant proteins		
Manual Assay RNAscope Mm-Igf1-C1	ACD Bio	Mm-Igf1-C1
Manual Assay RNAscope Mm-Vip-C2	ACD Bio	Mm-Vip-C2
Manual Assay RNAscope Mm-tdTomato-C2	ACD Bio	Mm-tdTomato-C2
Manual Assay RNAscope Mm-Vip-C3	ACD Bio	Mm-Vip-C3
Manual Assay RNAscope Mm-Gad1-C3	ACD Bio	Mm-Gad1-C3
Opal 690	Akoya Biosciences	FP1497001KT
Tetrodotoxin (TTX) citrate	Alomone Labs	T-550
D-amino-5-phosphonovaleric (AP5) acid	Abcam	ab120003
Critical commercial assays		
RNAscope Multiplex Fluorescent Reagent Kit	ACD Bio	320850
RNAscope Multiplex Fluorescent Reagent Kit v2	ACD Bio	323110
Deposited data		
ChIP-seq data	This paper	GSE210656
Meso-seq data (cKO)	This paper	GSE227382
Meso-seq data (Kir2.1)	This paper	GSE227342
Experimental models: Organisms/strains		
Mouse: C57BL/6J	Envigo (Israel)	Order code 057
Mouse: Vip-IRES-FlpO	The Jackson Laboratory	RRID: IMSR_JAX: 028578
Mouse: Vip-IRES-Cre	The Jackson Laboratory	RRID: IMSR_JAX: 010908
Mouse: CAG-Sun1/sfGFP (INTACT)	The Jackson Laboratory	RRID: IMSR_JAX: 021039
Mouse: Igf1-E1-flox	This paper	N/A
Mouse: Igf1-E2/3-flox	This paper	N/A
Mouse: Igf1-E12/3-flox	This paper	N/A
Recombinant DNA		
pGL4_11_Nued2	Gift from Dr. M. Greenberg	RRID: Addgene_59744
pGL4.74[hRluc/TK]	Promega	E6927

(Continued on next page)

Continued

REAGENT or RESOURCE	SOURCE	IDENTIFIER
pGL4.11_Nued2_E1	This paper	RRID: Addgene_203830
pGL4.11_Nued2_E2	This paper	RRID: Addgene_203831
pGL4.11_Nued2_E3	This paper	RRID: Addgene_203832
pGL4.11_Nued2_E4	This paper	RRID: Addgene_203833
pGL4.11_Nued2_E5	This paper	RRID: Addgene_203834
pGL4.11_Nued2_E1_dAP1	This paper	RRID: Addgene_203835
pGL4.11_Nued2_E1_dAP2	This paper	RRID: Addgene_203836
pGL4.11_Nued2_E1_dAP1-2	This paper	RRID: Addgene_203837
pAAV-Ef1a-fDIO-GCaMP6s	Gift from Rylan Larsen	RRID: Addgene_105714
pAAV-Syn1-fDIO-mScarlet-KASH-2a-Cre	This paper	RRID: Addgene_203838
pAAV-Syn1-fDIO-mScarlet-KASH-2a-dCre	This paper	RRID: Addgene_203839
pAAV-hSyn-Kir2.1WT-2A-mScarlet-KASH	This paper	RRID: Addgene_203840
pAAV-hSyn-Kir2.1Mut-2A-mScarlet-KASH	This paper	RRID: Addgene_203841
pAAV-Ef1a-fDIO-eGFP-2A-Cre-WPRE	This paper	RRID: Addgene_203842
pAAV-Ef1a-fDIO-eGFP-WPRE	This paper	RRID: Addgene_203843
pAAV-Ef1a-fDIO-mRuby3-2A-Cre	This paper	RRID: Addgene_203844
pAAV-Ef1a-fDIO-mRuby3-2A-dCre	This paper	RRID: Addgene_203845
pLenti-hUbc-Cre-GFP	Gift from Dr. Pascal Kaeser	N/A
pLenti-hUbc-dCre-GFP	Gift from Dr. Pascal Kaeser	N/A
Software and algorithms		
MATLAB	MathWorks	N/A
pClamp	Molecular Devices	N/A
LabVIEW	LabVIEW	N/A
GraphPad Prism	GraphPad Software Inc.	N/A
R	RStudio	N/A

RESOURCE AVAILABILITY

Lead contact
Further information and requests for resources and reagents should be directed to and will be fulfilled upon reasonable request by the lead contact, Ivo Spiegel (ivo.spiegel@weizmann.ac.il).

Materials availability
The plasmids newly created in this study are available from Addgene.

Data and code availability
ChIP-seq and RNA-seq data have been deposited at GEO (Superseries accession number GSE210658). This paper did not report original code. Any additional information required to reanalyze the data reported in this paper is available from the lead contact upon reasonable request.

EXPERIMENTAL MODEL AND SUBJECT DETAILS

Animals and dark-housing/light-exposure (DH/LE) sensory stimulation paradigm
All procedures involving animals were reviewed and approved by the Weizmann Institutional Animals Care Committee. Experiments were done in young adult mice of either sex, housed up to five animals per cage in a 12/12 dark/light cycle. All mice used in this study were heterozygous for Vip-IRES-FlpO and homozygous for any cKO allele or heterozygous for Vip-IRES-Cre and the INTACT allele ("Vip-Cre::INTACT").

For DH/LE sensory stimulation, mice were dark-housed for 10-14 days in light-sealed cabinets and the cages were refreshed once after 3-5 days in the dark using night goggles. Light exposure was performed in the same cabinets with LEDs providing ambient light situated above the cage for one or twelve hours after which the mice were sacrificed and the tissue was dissected. Animals that were not light-stimulated were enucleated in the dark with night goggles prior to dissecting the tissue.

METHOD DETAILS

Neuronal cell cultures

Primary neuronal cultures were prepared from E16 embryonic mouse cortices (mixed cultures) or E14 embryonic cortices (excitatory, EXC) and medial ganglionic eminences (inhibitory, INH) essentially as described.[17] In brief, tissues were dissected and then dissociated for 5-10 min in dissociation medium (HBSS, MgCl$_2$·6H$_2$O 10mM, Sigma), HEPES (10 mM, Sigma), kynurenic acid (1.25 mM, pH 7.2, Sigma) containing 200 μg/mL papain (Roche) and 0.32 mg/mL l-cysteine (Sigma). Papain treatment was halted by washing dissociated cells three times in dissociation medium consisting of 1 mg/mL trypsin inhibitor and bovine serum albumin (Sigma) and one more time with 10 mg/mL trypsin inhibitor and bovine serum albumin. Finally, three more washes with neuronal growth medium (Neurobasal medium; ThermoFisher), supplemented with B27 (2%; Thermo Fisher), Penicillin/Streptomycin (Life Technologies) and GlutaMAX (1 mM; ThermoFisher)). Cells were then triturated using a one mL pipette to achieve a single cell suspension. After dissociation, neurons were kept on ice until plating. Cell culture surfaces were coated overnight with 0.1 mg/mL poly-D-lysine (Sigma) and 10 μg/mL mouse laminin (Sigma), washed three times with sterile distilled water and left to dry at 37°C in an incubator. Cells were then plated at the desired cell density and placed in a cell culture incubator (37°C, 5% CO^2) for one and a half to three hours. Finally, the medium was completely aspirated and replaced with fresh pre-warmed neuronal growth medium.

For assessing activity-dependent gene expression profiles in neurons, *in vitro day* 6 neurons were silenced overnight with TTX (1 μM) and AP5 (100 μM). The next morning, neurons were either left silenced (unstimulated) or were stimulated for 1-6 hours with KCl (55 mM).

H3K27Ac ChIP-seq from cultured inhibitory and excitatory neurons

Inhibitory and excitatory neurons were cultured for 6 days, silenced overnight with TTX (1 μM) and AP5 (100 μM), and harvested on the next day (DIV 7) before or after depolarization for 2 hours with 55 mM KCl. 1-2 million neurons were used per ChIP-seq sample. ChIP-seq (Chromatin-immunoprecipitation followed by high-throughput sequencing) was performed essentially as described[36,37] using an antibody against acetylated Lysine 27 on Histone 3 (H3K27Ac; Abcam ab4729). Immunoprecipitated DNA fragments were repaired following the End-It DNA End Repair Kit (Epicentre biotechnology) manufacturer's instructions. The repaired ChIP DNA fragments were purified by the MinElute Reaction Cleanup Kit (Qiagen) and eluted in 20 ml of EB buffer. The cleaned up ChIP DNA fragments were sent to BGI China for library construction and sequencing. A minimum of 20 million reads were obtained for each library.

Cloning of DNA constructs

Cloning of all constructs was done using standard cloning techniques, and the integrity of all cloned constructs was validated by DNA sequencing.

The enhancer reporter plasmids were generated from pGL4.11_Nued2 plasmid (Addgene #59744) that contains a multiple cloning site about 3kb upstream of the firefly luciferase gene (2.4 kb upstream of a minimal promoter[37]). SbfI and AscI (NEB) were used to digest the plasmid and the T4 Ligase (NEB) inserted each genomically PCR amplified enhancer region. The E1 AP1 KO sequences were generated by PCR and cloned into pGL4.11_Nued2 plasmid using Gibson cloning (NEB).

The viral constructs pAAV-Syn1-fDIO-mScarlet-KASH-2a-Cre (and dCre) were generated on the backbone of pAAV-Ef1a-fDIO-EYFP (Addgene #55641) using NEBuilder HiFi DNA Assembly Master Mix (NEB, E2621L). The mScarlet-KASH (from pAAV-CAG-DIO-mScarlet-KASH, a generous gift from Dr. Ofer Yizhar, Weizmann Institute of Science) was inserted instead of the EGFP and included a 2A sequence. The Syn1 sequence (from pLenti-hSyn-Cre-GFP) was first combined with Cre or dCre using Gibson cloning and was then used to replace the Ef1a promoter while in parallel inserting the frt flanked Cre or dCre behind the 2a sequence.

To generate Flp-dependent eGFP-2A-Cre and EGFP constructs, we used pAAV-Ef1a-fDIO-eYFP (Addgene plasmid #55641) as a backbone and replaced the eYFP with either an eGFP-2A-Cre or an eGFP cassette. AscI and NheI-HF (NEB) were used to digest the plasmid and the T4 Ligase (NEB) inserted each cassette. This strategy yielded plasmids termed pAAV-Ef1a-fDIO-eGFP-2A-Cre-WPRE and pAAV-Ef1a-fDIO-eGFP-WPRE. We used the same backbone to generate Flp-dependent mRuby3-2A-Cre and mRuby3-2A-dCre constructs, by replacing the eYFP with either a mRuby3-2A-Cre or a mRuby3-2A-dCre cassette. AscI and BsrGI-HF (NEB) were used to digest the plasmid and the T4 Ligase (NEB) inserted each cassette. This strategy yielded plasmids termed pAAV-Ef1a-fDIO-mRuby3-2A-Cre and pAAV-Ef1a-fDIO-mRuby3-2A-dCre.

The AAV constructs pAAV-Syn1-Kir2.1-T2A-mScarlet-KASH (and Kir2.1mutant) were generated on the backbone of pAAV-W3SL-hSyn1-fDIO-MCS (generated based on Addgene #61463; digested with BspEI and EcoRI) using NEBuilder HiFi DNA Assembly Master Mix (NEB, E2621L). The mScarlet-KASH (from pAAV-Syn1-fDIO-mScarlet-KASH-2a-dCre, generated in this study) was inserted together with the Kir21-T2A sequences (from pCAG-Kir2.1-T2A-tdTomato, Addgene #60598; pCAG-Kir2.1Mut-T2A-tdTomato, Addgene #60644).

Luciferase assay

Separate inhibitory and excitatory cultures were grown on a 96-well plate at a density of 100 thousand cells/well. On day *in vitro* 6, cells were co-transfected with a total of 250 ng of plasmid DNA per well consisting of the luciferase reporter plasmid (178 ng/well), an internal control plasmid expressing renilla (36 ng/well; pGL4.74, Promega) and an empty backbone (36 ng/well, pBluescript II SK(+), Stratagene). All conditions consisted of three technical replicates on the same plate. Three days post-transfection, half of the wells

were depolarized as described above for five hours and the cells were harvested following the manufacturer's instruction of the dual-luciferase reporter assay system (Promega). The luciferase and renilla signal per well was measured according to the manufacturer's instructions on a microplate reader with dual-syringe injectors (Biotek SynergyH1).

In order to compare differences between wells/conditions, the luciferase signal for each well was divided by the signal from the internal control renilla to obtain a normalized luciferase value and averaged across the technical replicates. Technical replicates that contained very little renilla signal (luminance<25) were excluded from the analysis. In order to compare the data across biological replicates, the data were normalized within each experiment to the stimulated pGL4.11_Nued2_E1 condition, which was set to 1.

Generation of cKO animals

The Igf1-E1 cKO mouse was generated on a C57BL/6J background by Cyagen Biosciences Inc using standard techniques and protocols for homologous recombination in ES-cells. The targeting vector was engineered by PCR amplification of BAC clone RP23-363J14 or RP23-214M15 from the C57BL/6J library in which E1 is flanked by LoxP sites and additionally included a Neo cassette flanked by Frt sites for negative selection. Correctly targeted ES-cells were confirmed via Southern blotting and subsequently selected clones for blastocyst microinjection to generate chimera founders. Chimera founders were crossed with C57BL/6J mice to generate F1 heterozygous mutant mice.

The Igf1-E2/3 and Igf1-E12/3 cKO mice were generated using CRISPR/Cas9 technology in order to insert two Lox2722 sequences flanking both E2 and E3 together. Two separate sgRNAs (specific to the E2/3 up-stream and down-stream sites) were delivered to the embryo together with the spCas9 protein (IDT, 1081058) and two ssHDR DNA oligo's (total length of 160bp) with homologous arms (57-60bp) to the specific region. The Igf1-E2/3 cKO mutant was generated on a C57BL/6J background, while the Igf1-E12/3 double cKO mutant was generated on the background of the Igf1-E1 mutant mice. PCR verified chimera founders were crossed to C57BL/6J mice to generate F1 heterozygous mutant mice.

Lentiviral production

Lentiviral particles were produced essentially as described.[17] HEK293T cells were grown in DMEM supplemented with 10% heat-inactivated FBS and penicillin-streptomycin (Life technologies). The day before transfection, cells were plated on 10 cm culture dishes (8-10 dishes) coated with Poly-L-Lysine at a density of four million cells. Cells were then transfected with pMDL-GP-RRE (5 μg), pCMV-VSV-G (2.5 μg), pRSV-Rev (2.5 μg) and 25 μg of the expression plasmid for Cre or dCre (Ubc-CreGFP, Ubc-dCreGFP) using the calcium-phosphate method. After two days, the medium was collected and stored at 4°C and replaced by fresh growth medium. On the third day the medium was collected and combined with the medium of day two, sterile-filtered (0.45 μm filter) and centrifuged at 25,000 x G for two hours in order to pellet the lentivirus. The supernatant was then aspirated and replaced with 100 μl Neurobasal medium. The viral pellet was gently resuspended on a shaker at 4°C overnight. Concentrated virus was used directly or stored at -80°C until use. On *in vitro* day three 10% of the final concentrated solution was used to infect a 24-well plate consisting of ~400,000 cells/well.

AAV production

AAV particles were produced as described.[27,73] HEK293T (ATCC) cells were grown in DMEM supplemented with 5% FBS, penicillin-streptomycin (Life Technologies), NEAA (11140050, Gibco™) and sodium pyruvate (1mM; 03-042-1B, BI) and were plated the day before transfection at a density of 12 million cells on 15cm poly-L-lysine coated plates. On the next day, equal amounts of the pDJ, pHelper and the expression cassette (13.33 μg each) were transfected using PEI. Two days post-transfection, the medium containing the released AAV virions was stored at 4°C and replaced with fresh medium for an additional two days. Five days post transfection, the cells and medium were collected for purification. PEG was used to precipitate AAV particles in the medium and subsequently added to the cell lysate. Using a salt active nuclease (SRE0015, Sigma), the cells were lysed to release the AAV and were pelleted by centrifugation. The supernatant was loaded onto an iodixanol gradient and centrifuged for 2.25 h at 59.000 RPM (70 Ti rotor) in an ultracentrifuge. 4-5 mL were collected from the clear 40% layer containing the AAV and further concentrated using Amicon filters to the desired volume. AAV titers were estimated using qPCR, after which the AAVs were aliquoted and kept at −80°C for long-term storage.

Stereotactic intra-cortical injections of AAV constructs

Animals were anesthetized by isoflurane and secured in the stereotactic apparatus (Kopf Instruments, model 942) on a heating pad maintained at 37°C. Before the surgical procedure, local anesthesia (2% Lidocaine) was injected under the scalp and ophthalmic ointment (Duratears) was applied to the eyes. The scalp was cleaned with 70% ethanol and betadine three times before incision and exposure of the skull. The visual cortex was estimated by stereotactic coordinates (2.7 mm posterior and 2.5 mm lateral from bregma) and burr holes were drilled through the skull. A glass pipette filled with AAV particles was inserted to a depth of 300-400μm to reach layer 2/3 of the cortex. Two minutes after penetrating the brain, 300 nl was injected at a rate of 65 nl/min. Two minutes post-injection the pipette was retracted and repeated up to a total of six injections (three in each hemisphere). After the injections, the scalp was closed with Vetbond (3M) and the mice were given Buprenorphine (0.1 mg/kg) and carprofen (5 mg/kg). After initial recovery on a heating pad (RWD Life science), the mice were returned to their homecage and subsequently monitored for three consecutive days with additional injections of carprofen.

Meso-seq

FACS-based isolation of (50–100) visual cortex nuclei and RNA-seq was performed following the Meso-seq method as described previously.[54] Briefly, frozen tissue was homogenized in a precooled two mL dounce homogenizer containing freshly prepared homogenization buffer (10 mM Tris pH 8.0, 250 mM sucrose, 25 mM KCl, 5 mM MgCl2, 0.1 % Triton-X 100, 0.5% RNasin Plus RNase inhibitor (Promega), 1X protease inhibitor (Promega), and 0.1 mM DTT). The homogenate was pelleted by centrifugation and resuspended in a staining buffer (1X PBS, 0.8% nuclease-free BSA and 0.5% RNAsin Plus RNase inhibitor). DAPI was added in order to detect nuclei and exclude debris and doublets. For each animal total nuclei (DAPI+) or AAV expressing nuclei (DAPI+ & mScarlet+) were sorted directly into lysis buffer (0.2% Triton X-100 in ddW, dNTPs, Oligo-dT30VN primers, ERCC & RNAse inhibitors). Isolated nuclei were frozen at -80°C until library preparation.

RNA-seq libraries were prepared at the Crown Genomics Institute of the Nancy and Stephen Grand Israel National Center for Personalized Medicine (G-INCPM) of the Weizmann Institute of Science. Reverse transcription was performed directly on the isolated nuclei, followed by PCR-amplification (17 cycles) and cDNA cleanup with Agencourt Ampure XP beads (Beckman Coulter). The cDNA libraries were generated using Nextera XT (Illumina) and sequenced on a NextSeq 500 sequencer (Illumina, 75bp single-end reads).

RNAscope fluorescence in situ hybridization (FISH)

FISH was done with the RNAscope systems (Advanced Cell Diagnostic) following manufacturer's instructions. For assessing *Igf1* expression in cultured neurons, mixed cortical cultures were prepared and stimulated as described above while on coated glass coverslips. Pretreatment and FISH were done following the RNAscope Fluorescent Multiplex Assay with probes against Igf1 (mm-Igf1-C1), Vip (mm-Vip-C2) and Gad1 (mm-Gad1-C3). Images were taken on a confocal microscope (Zeiss LSM800).

For FISH in acute brain slices, brain tissues were freshly dissected and frozen in OCT compound (TissueTek, #4583). Coronal sections (15 μm thick) of visual cortex expressing AAV were cut using a Leica CM1950 cryostat and mounted on SuperFrost Plus glass slides (Fisher Scientific). Pretreatment and FISH were performed following the RNAscope Fluorescent Multiplex Assay with probes against Igf1 (mm-Igf1-C1), tdTomato (mm-tdTomato-C2) and Vip (mm-Vip-C3).

For FISH in fixed brain slices, anesthetized (10% ketamine and 1% xylazine in PBS) animals were transcardially perfused with 5 ml of ice-cold PBS and subsequently 15 ml of cold fixative (4% PFA in PBS). Brains were then dissected, post-fixed (in 4% PFA) for 3 hours on a rotator at 4°C and afterwards washed three times in cold PBS. Brains were left overnight in 30% sucrose at 4°C and subsequently frozen in OCT compound (TissueTek, #4583). Coronal sections (15 μm thick) were prepared as described above and stored at -80°C until use. Before starting the FISH protocol, slides were briefly thawed and immediately taken to a confocal microscope (Zeiss LSM800) in order to image the mRuby fluorescence. Afterwards, slides were pretreated for FISH by heating at 99°C for 5 min, dehydrated in 100% ethanol and underwent protease treatment. Hybridization, amplification and conjugation with Opal 690 (Akoya Biosciences, FP1497001KT) of the VIP probe (mm-Vip-C1) were done following the RNAscope Fluorescent Multiplex Assay v2 manufacturers instructions. Confocal images were taken at the same location as the images taken before the FISH. The two images were then overlapped in order to assess the expression of mRuby in VIP INs.

FISH images were analyzed in Matlab using custom-built scripts to quantify the number of *Igf1* puncta present per nucleus. For the analysis of cKO of Igf1 enhancers, only the VIP INs with the highest number of viral mRNA puncta per condition (top 10%) were considered.

Immunohistochemistry

Animals were transcardially perfused with 5 ml of ice-cold PBS and subsequently 15 ml of cold fixative (4% PFA in PBS). Brains were then dissected, post-fixed (in 4% PFA) for 1 hour on a rotator at 4°C and afterwards washed three times in cold PBS. Brains were left overnight in 30% sucrose at 4°C and subsequently frozen in OCT compound (TissueTek, #4583). Coronal sections (10 μm thick) of AAV infected visual cortex tissue were cut using a Leica CM1950 cryostat and mounted on SuperFrost Plus glass slides (Fisher Scientific). The slices were then washed in PBS and incubated for 1 hour in a blocking solution (1x PBS, 10% NGS, 0.5% Triton-X). The blocking buffer was then replaced with the Rabbit-anti-VIP antibody (ImmunoStar, 20077) diluted in the blocking buffer (1:1000) and left at 4°C for 60 hours. The slides were then washed in PBS and incubated for 1 hour at room temperature with Goat-anti-rabbit Alexa 488 (Molecular Probes, A-11039) diluted 1:1000 in a blocking buffer (1x PBS, 10% NGS, 0.3% Triton-X) with a nuclear stain (DAPI). Slides were mounted with Fluoromount-G (SouthernBiotech, 0100-01) and imaged on a confocal microscope (Zeiss LSM800).

Patch-clamp electrophysiology in acute visual cortex slices

P60-80 mice were transcardially perfused with ice-cold sucrose dissection media (26 mM NaHCO$_3$, 1.25 mM NaH$_2$PO$_4$, 2.5 mM KCl, 10 mM MgSO$_4$, 11 mM glucose, 0.5 mM CaCl$_2$, 234 mM sucrose; 340 mOsm). Brains were then dissected and sliced, while being kept in ice-cold sucrose dissection media, into coronal sections (300 μm thick) containing the primary visual cortex using a Leica VT1200S vibratome. Slices were incubated in high osmotic concentrated artificial cerebrospinal fluid (28.08 mM NaHCO$_3$, 1.35 mM NaH$_2$PO$_4$, 132.84 mM NaCl, 3.24 mM KCl, 1.08 mM MgCl$_2$, 11.88 mM glucose, 2.16 mM CaCl$_2$; 320 mOsm) at 32°C for 30 minutes immediately after slicing. Then, slices were incubated in normal osmotic concentrated artificial cerebrospinal fluid (26 mM NaHCO$_3$, 1.25 mM NaH2PO$_4$, 123 mM NaCl, 3 mM KCl, 1 mM MgCl$_2$, 11 mM glucose, 2 mM CaCl$_2$; 300 mOsm) at 32°C for 30 minutes and subsequently at room temperature. All solutions were saturated with 95%-O2/5%-CO$_2$, and slices were used within 6 hours of preparation. Whole-cell patch-clamp recordings were performed in aCSF at 32°C from neurons in the visual cortex

that were identified under fluorescent and DIC optics. Recording pipettes were pulled from borosilicate glass capillary tubing with filaments (OD 1.50 mm, ID 0.86 mm, length 10 cm) using a P-1000 micropipette puller (Sutter Instruments) and yielded tips of 2–5 MΩ resistance. Recordings were sampled at 20 kHz and filtered at 3 kHz.

All mPSC experiments were recorded in a voltage patch-clamp mode and with pipettes filled with an internal solution containing: 135 mM caesium methanesulfonate, 4 mM TEA-Cl, 10 mM HEPES, 1 mM Mg-ATP, 0.3 mM Na-GTP, 10 mM phosphocreatine (Tris), and 3 mM QX-314-Cl. Osmolarity and pH were adjusted to 310 mOsm and 7.3 pH with sucrose and CsOH, respectively. mEPSCs were isolated from mIPSCs by exposing neurons to 0.5 μM tetrodotoxin (TTX) and holding them intermittently at −70 mV or 0 mV, respectively, as previously described.[74] All intrinsic properties experiments were recorded with pipettes filled with an internal solution containing: 135 mM potassium gluconate, 4 mM KCl, 10 mM HEPES, 4 mM Mg-ATP, 0.3 mM Na-GTP, Na_2-ATP, and 10 mM phosphocreatine (Tris). Osmolarity and pH were adjusted to 310 mOsm and 7.2 with sucrose and KOH, respectively. Intrinsic properties were measured in current-clamp mode using both a ramp and steps protocols, as previously described.[75] In all whole-cell patch-clamp recordings, either a green or red fluorophore was added to internal solutions to dye-fill neurons (2.73 μM of either CF-488A hydrazide or CF-594 hydrazide, respectively; Sigma-Aldrich).

Data were acquired via Clampex10 using a Multiclamp 700B amplifier and digitized with an Axon Digidata 1550B data acquisition board (Axon Instruments).

In vivo 2-photon imaging

Viral injections and cranial window implantations for 2-photon imaging

~P60 mice were anesthetized with isoflurane at an initial concentration of 4% and a maintenance level of 1.5-2%. The mice were fixed in a stereotactic apparatus (Kopf Instruments, model 942) and ophthalmic ointment (Duratears) was applied to the eyes. Body temperature was kept at 37°C with a heating blanket (RWD Life science). Before the surgical procedure, local anesthesia (2% Lidocaine) was injected under the scalp and the skin was scrubbed with 70% ethanol and betadine. For imaging experiments, a 4 mm craniotomy above the visual cortex was made and following the viral injection, a cover glass was glued to the skull using VetBond (3M) and a custom-made head-post was glued to the skull (Krazy glue). Following surgery, the animals were administered with analgesics (0.1 mg/kg of buprenorphine and 5 mg/kg of Carprofen).

Eyes suturing

To minimize light stimulation of the retina throughout imaging of the spontaneous activity of VIP INs in dark-housed mice, eyelids of both eyes were trimmed and sutured under isoflurane anesthesia (1–2% in O_2), prior to dark-housing, as previously described.[76]

In vivo 2-photon calcium imaging and pupillometry

2-photon imaging: Imaging was performed at least 3 weeks after AAV injections using a two-photon microscope with a 12 kHz resonant-galvo scanhead (Bergamo microscope, ThorLabs) at an acquisition rate of about 11Hz at a single plane. Frame size was 512 x 512 pixels and images were acquired at three different z-planes using a fast piezo motor (Thorlabs). Illumination was provided by a Mai Tai DeepSee laser at 930nM. Pupillometry: During imaging, the mouse's ipsilateral eye was illuminated with an IR-light source (M940L3, Thorlabs) and imaged using a CMOS camera at 33 Hz.

Visual stimulation

Visual stimuli were created using Matlab with Psychophysics Toolbox (http://psychtoolbox.org/) and presented on a gamma corrected LCD screen. The monitor was positioned 20 cm (imaging) from the contralateral eye of the recorded hemisphere, covering 100° horizontally and 85° vertically of the mouse's visual field. The monitor was placed at the center of the receptive field of the majority of the imaged neurons, as determined prior to the experiment by performing receptive field mapping by presenting circular patches of drifting sinusoidal gratings (set to 25 degrees) spacing on a 3 by 4 grid. Stimuli were presented for 1 second at the four cardinal directions with an interstimulus interval of 4 sec in which a grey screen of mean luminance was presented. For imaging experiments, full field sinusoidal drifting bar gratings with a temporal frequency of 2 Hz, 100% contrast and varying spatial frequencies (0.01, 0.04, 0.1, 0.15 and 0.3 cpd) were displayed in 8 directions evenly spaced in a pseudorandom order. Stimulus presentation duration was 2 seconds long, and inter-stimulus interval was 5 seconds long during which a grey screen of mean luminance was displayed. A minimum of 10 up to 15 repetitions were presented per stimulus.

During Ca^{2+} imaging session, when spontaneous activity was recorded and no visual stimuli were presented, a grey screen of mean luminance was displayed.

Data analyses

H3K27Ac ChIP-seq analysis

The H3K27Ac ChIP-seq libraries from cultured neurons were sequenced and demultiplexed at BGI Genomics. The *in vivo* H3K27Ac ChIP-seq libraries from VIP INs in the visual cortex were downloaded from the GEO (GSM4551847, GSM4551848, GSM4551849, GSM4551850). All the libraries contained at least 15 million reads. Illumina adaptors were removed using Cutadapt[77] (v1.18) and reads were trimmed from 3' end until the final base had a quality score > 30, discarding reads left with < 36 bp. The resulting reads were aligned to the UCSC mm10 genome using Bowtie2[78] (v2.3.3) with –no-mixed –no-discordant. A sorted and indexed BAM file (acquired using Samtools[79,80] v1.9) was used to call broad peaks with MACS3[81] (v3.0.0a7) using default settings. Since the

signal-to-noise is relatively low in the *in vivo* libraries, the default cut-off q-value becomes too stringent and many peaks will fail to pass the threshold. We therefore performed a cut-off analysis with MACS3 (–cutoff-analysis) and determined that a cut-off p-value of 0.01 was best suited for calling broad peaks for these libraries.

Differential binding analysis was performed using the R package DiffBind[82] (v3.6.2). A consensus peak-set for each experiment was generated containing peaks that were present in all biological replicates per condition with a summit size of 500 bp for cultured neurons and 1500 bp for the *in vivo* dataset, which contained significantly broader peaks compared to the dataset from cultured neurons. In both cases, Deseq2 determined the differential binding of H3K27Ac at genomic sites for each cell-type and between stimulation conditions (FDR < 0.05).

In order to annotate peaks to genes and genomic features we used the R package ChIPseeker[83] (v1.32) in combination with the UCSC gene annotation database (TxDb.Mmusculus.UCSC.mm10.knownGene v3.10, Bioconductor) and genome-wide mouse annotation (org.Mm.eg.db v3.15, Bioconductor). Peaks were assigned to the nearest genes and classified as promoters (-1000 or +500 from TSS).

Motif enrichment analysis was performed using the findMotifsGenome (-size option was set to 1,000) function in Homer[84] (v4.9.1) for activity-dependent enhancers (intra- and inter-genic regions) and promoters separately. The peaks in the resulting categories were then divided into regulated (enhancer or promoter) peaks enriched for a given cell-type (inhibitory or excitatory) or regulated peaks that were shared between them. The peak-set used as background for estimating motif enrichment consisted of all H3K27Ac peaks found in the consensus peak-set generated by DiffBind. The number of regulated peaks with canonical AP-1 motifs were counted using annotatePeaks.pl with a motif file generated with seq2profile.pl (TGACTCA and/or TGAGTCA; Homer v4.9.1).[84] Known TFBS in the Igf1 enhancers were retrieved from the JASPAR database.

ATAC-seq analysis

The *in vivo* ATAC-seq libraries from cortical VIP INs were downloaded from GEO (GSM1541968, GSM1541969). Illumina adaptors were removed using Cutadapt[77] (v1.18) as described before in the H3K27Ac ChIP-seq analysis. The resulting reads were aligned to the UCSC mm10 genome using Bowtie2[78] (v2.3.3) with –very-sensitive –no-mixed –no-discordant -I 10 -X 2000. Duplicate reads were removed using Picard (v2.25.5, Broad Institute) and peaks were called with the remaining reads using MACS3[81] (v3.0.0a7) with the settings –nomodel –broad –shift -75 –extsize 150. In order to find genomic sites with peaks present in both biological replicates, the R package DiffBind[82] (v3.6.2) was used by generating a consensus peakset as done before.

FOS Cut & Run analysis

The Cut & Run data for FOS in KA stimulated cortical VIP INs were downloaded from GEO (GSM4551863, GSM4551867). Adapters were trimmed using Cutadapt[77] (v1.18) with -q 20 -p 10 -m 10 and subsequently aligned using Bowtie2[78] (v2.3.3) with -local -very-sensitive-local -no-unal -no-mixed –no-discordant -I 10 -X 700. Narrow peaks were called using MACS3[81] (v3.0.0a7) with default settings. Significant binding for both replicates was assessed as before with the R package Diffbind[82] (v3.6.2).

Meso-seq analysis

RNA-seq data obtained with the Meso-seq method was sequenced at a depth of ~5-10 million reads and were preprocessed as described previously.[54] Briefly, Cutadapt[77] (v1.18) was used to remove illumina adaptors from the raw (fastq) reads and the 3' ends were trimmed until the final base had a quality score > 20, discarding reads left with < 25 bp. The reads passing this quality filter were aligned to the UCSC mm10 mouse genome using STAR[85] (v2.5.3a) and a raw gene expression count matrix was generated with Homer[84] (v4.9.1) which included both intronic and exonic reads. Genes were considered as expressed in a condition based on the following criteria: (1) at least 3 samples will have more than 10 reads, (2) with a coefficient of variance below 0.5. Only genes that were expressed in ~10% or more of the total number of conditions per experiment were used for normalisation (median of ratios method) and were subsequently used for enrichment analyses.

Differential gene expression analysis was performed using the R package Deseq2[86] (v1.36) for each nuclei population separately. The raw count matrix for a given population was filtered based on the criteria described above (cKO: infected-VIP - 12,241 genes, non-infected nuclei - 13,756 genes; Kir2.1: VIP - 10688 genes) and normalized by genes that were considered expressed in at least 6 out of 12 conditions in the cKO experiment (VIP - 5,762 genes; non-infected nuclei - 9,282 genes) and in all conditions for the Kir2.1 experiment (VIP - 4035 genes). The Likelihood-ratio test was used to identify genes significantly regulated by light-stimulation and genes that showed a significant interaction between the cKO and light-stimulation. Pairwise comparisons between groups for specific genes were calculated using the Wald-test.

Analysis of electrophysiological recordings

To ensure data quality, recordings were included only when they were acquired with an access resistance below 20 MΩ. mPSCs events were automatically detected and characterized with custom MATLAB scripts using the functions abfload and iPeak from MATLAB Central File Exchange. The charge was calculated as the area under the curve of each single mPSC event (i.e., only areas under curves of detected events were used for the calculation of the charge). The starting and ending points of an event were determined as the nearest time points before and after a peak where the value of the measured current was lower than 10% of the value of the event's amplitude. The E/I-ratio was calculated based on the average charge of mPSCs, as follows:

$$E \Big/ I \; Ratio = \frac{C_{mEPSCs} \; - \; C_{mIPSCs}}{C_{mEPSCs} + C_{mIPSCs}}$$

The average mPSCs charge was calculated as the average sum of current along one second of recording (as 1 Coulomb = 1 Ampere · 1 Second). All data were analysed blind to genotype or experimental conditions. Statistical tests were performed using GraphPad Prism. Intrinsic properties were automatically extracted and calculated by custom MATLAB scripts using the abload function from MATLAB Central File Exchange. Mann-Whitney test was used for paired comparisons. In the case of multiple comparisons, post-hoc Dunnett's T3 multiple comparisons test was performed following a Brown-Forsythe ANOVA test.

Analysis of Ca²⁺ 2-photon imaging data

Unless otherwise mentioned, all recordings (i.e. Fluorescent (F) signals derived from 2-photon imaging) were analyzed using custom software written in MATLAB (The MathWorks). Raw calcium movies were analyzed using Suite2p.[87] Neuropil corrected signals were resampled to 100 Hz using a linear interpolation. For cross-correlation measurements, F signals were smoothed with a Savitzky–Golay filter with a first-order polynomial and a window size of 11 points. Cross-correlation coefficient (CC), at 0 time-lag, of spontaneous activity was calculated between all possible cell pairs per recording and between each cell and the calculated pupil diameter (see below) for a time window of 15 minutes (obtained in a separate imaging session). Shuffle correlations were computed as the correlation between each imaged cell and the inverse signal of the pupil or one of the cells in the cell-to-cell correlation. Visually evoked responses were calculated as the mean ΔF/F during visual stimulus presentation:

$$\Delta F \Big/ F = \frac{F - F0}{F0}$$

Baseline fluorescence (F0) was calculated as the mean fluorescence of the 1 second preceding the visual stimulus. The preferred direction was defined as the direction in which the gratings elicited the largest response. Preferred spatial frequency was determined as the spatial frequency that elicited the largest response at the preferred direction. To determine if a cell was significantly responsive to the drifting grating stimulus, a one-way non-parametric ANOVA (Kruskall-Wallis) was computed comparing the evoked responses to baseline fluorescence. Cells with a resulting p-value of <0.05 and a response of above 6% were called visually responsive.

Spontaneous activity rate was calculated from the deconvolved signal produced by the Suite2p algorithm. Walking periods (defined as periods when the treadmill speed was greater than 0.1 cm s⁻¹ after smoothing the treadmill signal) were removed for rate calculation.

Pupil diameter measurement

Pupil size was analyzed using custom software written in LabView (NI). Frames were filtered using a median filter and thresholded to low IR light reflectance areas. The resulting regions were then filtered based on circularity and size until only the region corresponding to the pupil remained, as verified manually during each analysis. Consequently, an ellipse was fitted to this region by setting its major and minor axes equal to the longer and shorter lines of symmetry of the bounding rectangle. The pupil diameter was estimated as the geometric mean of the major and minor axes.